J. Fluid Mech. (1979), *vol.* 95, *part* 3, *pp.* 431–464
Printed in Great Britain

On heating a stable salinity gradient from below

By HERBERT E. HUPPERT AND P. F. LINDEN
Department of Applied Mathematics and Theoretical Physics,
University of Cambridge

(Received 20 December 1978)

When heat is applied at the bottom of a stable salinity gradient a series of layers with uniform temperature and salinity is formed. The evolution of this system is investigated in the laboratory and a numerical model of the process is developed. New layers are formed sequentially at the top of a growing convection region while lower down adjacent layers merge. For given fluid properties the convection depends upon one parameter Q, which is proportional to the (suitably non-dimensionalized) ratio of the salinity gradient to the heat flux. We find that the depth of the top of the convecting region and the number of layers present increase like the square root of time over the range of Q examined. This permits the definition of an effective conductivity, K_T, for the total series of layers which is directly proportional to κ_T, the molecular thermal diffusivity, and inversely proportional to Q. The vertical growth of the layers is thus retarded by increasing Q. The average thickness of the layers decreases with increasing salinity gradient and appears to be independent of the applied heat flux.

1. Introduction

Double-diffusive convection occurs in a fluid with two (or more) components with different molecular diffusivities which contribute in opposing senses to the vertical density gradient. A hallmark of double-diffusive convection is the existence of layers separated by relatively thin interfaces. Due to turbulent convection the components are fairly uniform throughout each layer. In the interfaces there are strong property gradients and molecular diffusion is important.

In order to investigate many of the fundamental aspects of the motion in the layers or the transfer of properties through the interfaces it is often convenient to pre-set the layer depths, and many theoretical and experimental investigations have done this. Alternatively, a few different situations have been investigated in which the layer depths result directly from the double-diffusive process and have to be calculated or measured. The first example in the literature of this alternative approach is the qualitative experiment of Turner & Stommel (1964), followed by the quantitative investigation of Turner (1968).

The situation Turner & Stommel considered was the application of a heat flux to the bottom of a column of water stably stratified with salt. They observed that a turbulent mixed layer gradually built up from the bottom of the containing vessel. After some time a second layer was seen to form and grow above the first. At a later time a third layer appeared and so on. Turner argued that the first layer is the direct response to the applied heat flux and that ahead of its advancing front a thermal

0022–1120/79/4328–7800 $02.00

boundary layer is produced by molecular diffusion of heat. Both the temperature and the length scale of this boundary layer increase with time, until it eventually becomes unstable, breaks down and mixes to form the second layer. Parameterizing the instability by a Rayleigh-number criterion, Turner calculated the depth of the first layer at the time of formation of the second layer and carried out a series of experiments which compared favourably with his predictions. Turner did not continue either his calculations or quantitative experiments beyond this consideration of the first layer. However, it is clear from his paper that he believed the investigation of subsequent layers to be an important task which could be undertaken within the theoretical framework he had set up.

The aim of the present work is to carry out the necessary calculations and experiments to perform this task. A part of the motivation arises from the desire to compare the results of such an evolution calculation with oceanic layered temperature and salinity structure formed in the same way. Possible examples include the ice-covered portion of the Arctic Ocean (Neal, Neshyba & Denner 1969), Lake Vanda in Antarctica (Huppert & Turner 1972), Lake Kivu (Newman 1976) and the Red Sea (Degens & Ross 1969), the water column in the first example being cooled from above rather than heated from below. We anticipate considering this extension of our work in a subsequent paper.

In § 2 we present our interpretation of Turner's theory for the first layer, prior to explaining our theoretical extensions of his work in § 3. In this latter section the assumptions built into the theoretical model are put forward, the resulting equations are presented and the results of their numerical solution discussed. In § 4 we describe the experiments performed to test the theoretical model and in § 5 we present the experimental investigation of the various assumptions incorporated into the theoretical model. In § 6 the quantitative experimental results are compared with the theoretical results, and we find that the theoretical model satisfactorily describes the overall evolution and many of the details of the layer structure. In § 7 we argue that since the total depth of the layer structure increases as the square root of time, there is an effective (constant) conductivity which can be used to describe the advancing system of layers. A more general discussion and interpretation of the results then follows. The paper concludes with a short summary of the results of the entire investigation.

2. Turner's theory for the first layer

Consider a horizontally uniform, constant heat flux H applied from time $t = 0$ at the horizontal plane $z = 0$. Denote the initial, constant salinity gradient in the fluid occupying $z > 0$ by $d\bar{S}/dz$, which is negative. The buoyancy associated with the heat flux and the salinity gradient is incorporated by defining

$$H_* = -\alpha_0 g H/\bar{\rho}c, \quad S_* = -\tfrac{1}{2}\beta g d\bar{S}/dz, \tag{2.1a, b}$$

where α_0 is the (constant) coefficient of thermal expansion, β the analogous coefficient for salt, $\bar{\rho}$ a representative density of the fluid, g the acceleration due to gravity and c the specific heat. The remaining physical variables to be incorporated are the kinematic viscosity ν, the thermal diffusivity κ_T and the molecular diffusivity of salt, κ_S.

Any non-dimensional variable, say F, can then be expressed as

$$F = F(Q, \sigma, \tau), \tag{2.2}$$

where

$$Q = \kappa_T S_*/H_*, \tag{2.3}$$

$\sigma = \nu/\kappa_T$ is the Prandtl number and $\tau = \kappa_S/\kappa_T$ is the ratio of the diffusivities. Consideration of a heat/salt system specifies σ ($\simeq 7$) and τ ($\simeq 0{\cdot}01$) and there remains the one variable Q.

It is convenient now to define the non-dimensional variables

$$t = S_*^{\frac{1}{2}}\hat{t}, \quad z = H_*^{-\frac{1}{2}} S_*^{\frac{3}{2}}\hat{z}, \tag{2.4a, b}$$

$$T = -\alpha_0 g H_*^{-\frac{1}{2}} S_*^{-\frac{1}{2}}\hat{T}, \quad S = \beta g H_*^{-\frac{1}{2}} S_*^{-\frac{1}{2}}\hat{S}, \tag{2.4c, d}$$

where T and S represent temperature and salinity respectively and the circumflexed variables are dimensional. Throughout the remainder of the paper all quantities are non-dimensional, unless there is explicit indication to the contrary. In these non-dimensional terms the initial salinity gradient is -2.

We can now consider the growth of the first layer. In his paper, Turner made the following three assumptions. First, that the layer is well mixed and has uniform temperature T_1, and salinity S_1, over a depth h_1. Second, that the heat content of the thermal boundary layer ahead of the advancing front is small compared to that in the growing layer. Thus the loss of heat through the advancing front can be neglected in calculating the evolution of the first layer until the thermal boundary layer becomes unstable. Third, that the diffusion of salt can be neglected. The condition for the second assumption to be valid is that $Q \ll 1$ and for the third that $\tau \ll 1$. Conservation of heat and salt then yield

$$h_1 T_1 = t, \quad S_1 = -h_1. \tag{2.5), (2.6}$$

A third relationship is now needed. This comes from consideration of the dynamics at the top of the growing layer, in particular the mechanism of fluid entrainment. Turner discussed two extreme cases. If all the potential energy supplied by the heat flux is used to entrain fluid across the top interface $T_1 = -\frac{1}{3}S_1$. This limit, which predicts that a stable density step occurs across the top of the layer, neglects all dissipation and hence clearly it cannot be achieved in practice. The other extreme occurs if the density step across the top of the layer is zero. In this case

$$T_1 = -S_1. \tag{2.7}$$

Turner found from his experiments that this latter condition seems to be appropriate. The solution of (2.5)–(2.7) is

$$T_1 = -S_1 = h_1 = t^{\frac{1}{2}}. \tag{2.8}$$

Turner observed that after some time a second convecting layer forms above the first, halting its advance. He suggested that the formation of the second layer occurs when the thermal boundary layer ahead of the advancing top of the first layer becomes unstable. There is as yet no theoretical criterion known which characterizes the instability of such a time-dependent temperature profile. However, the criterion

for a fluid with constant temperature and salinity gradients confined between horizontal, stress-free conducting boundaries separated by a distance d has been extensively investigated. Linear stability theory, as detailed by Turner (1973), predicts that instability first occurs, in the form of an overstable oscillation for $\tau \ll 1$, when

$$R = R_T - \frac{\sigma}{\sigma+1} R_S \tag{2.9}$$

exceeds a critical value $R_c = 27\pi^4/4$. In this criterion, the (positive) thermal and saline Rayleigh numbers $R_T = -\alpha_0 g \Delta \mathsf{T} d^3/(\kappa_T \nu)$ and $R_S = \beta g \Delta \mathsf{S} d^3/(\kappa_T \nu)$ incorporate the temperature and salinity excesses $\Delta \mathsf{T}$ and $\Delta \mathsf{S}$ of the lower boundary over the upper one. Equating d to the thickness of the thermal boundary layer, Turner found that for his experiments concentrating on the evolution of the first layer $R_S \ll R_T$ and so used the stability criterion

$$R_T = R_c. \tag{2.10}$$

Assuming that once the stability criterion (2.10) is achieved the first layer immediately stops growing, Turner estimated that for $Q \ll 1$ the final depth of the first layer is given by

$$h_1 = \left(\frac{\sigma R_c}{64Q}\right)^{\frac{1}{4}}. \tag{2.11}$$

From a best fit to his experimental data obtained by visual observation of the depth of the first layer, Turner found that $R_c = (2{\cdot}4 \pm 0{\cdot}3) \times 10^4$.

A disquieting feature of this value for R_c is that it is approximately forty times larger than the value predicted by linear stability theory applied to time-independent basic profiles. One of the aims of this paper is to examine this criterion and in particular to ascertain whether it applies to the formation of the third and subsequent layers. In order to do this we need to incorporate in the model already described the heat and salt fluxes between layers. Experimentally determined flux laws obtained from measurements across a single interface between two convecting layers (Turner 1965; Huppert 1971) are used. The comparison of the model and the experiments will also indicate whether such flux laws are applicable when there are a number of coupled layers evolving with time.

3. The theoretical description of the evolution of many layers

Some of the assumptions incorporated in the theoretical model for the evolution of many layers are similar to those employed by Turner. These are:

(*a*) the model is one-dimensional;

(*b*) each layer is well mixed;

(*c*) the heat content of the thermal boundary layer ahead of the advancing front can be neglected in calculating the heat budget for the layers;

(*d*) the diffusion of salt across the advancing front can be neglected;

(*e*) the density step across the advancing front is zero;

(*f*) the criterion for the breakdown of the thermal boundary layer is (2.9); and

(*g*) the fulfilment of (2.9) indicates both the immediate cessation of the growth of what was the uppermost layer and the instantaneous initiation of another layer.

Assumption (*c*) implies that the total heat content of the water column is in excess of that put in at the bottom, though the percentage excess is slight if $Q \ll 1$. This assumption is a necessary feature of any one-dimensional model which is to predict an advancing (rather than receding) front and is discussed further below and in the appendix.

To these assumptions are added the following.

(*h*) Except for the process of layer merging, which is discussed in (*j*) below, only the uppermost layer has a depth which changes with time.

(*i*) The transfer of heat and salt through individual interfaces is specified by

$$\phi = 0{\cdot}32(Q/\sigma)^{\frac{1}{3}}(\Delta T)^{10/3}(\Delta S)^{-2} \tag{3.1}$$

and

$$\psi = (1{\cdot}85 - 0{\cdot}85R_\rho)\,\phi \qquad (1 < \Delta S/\Delta T \equiv R_\rho \leqslant 2) \tag{3.2a}$$

$$= 0{\cdot}15\phi \qquad (2 \leqslant R_\rho), \tag{3.2b}$$

where ϕ and ψ are the heat and salt fluxes through an interface across which there is a temperature difference ΔT and a salinity difference ΔS.

(*j*) If the density difference across an interface becomes zero ($\Delta T = \Delta S$), the two adjoining layers immediately merge to form one well-mixed layer whose heat and salt content is the sum of those for the two original layers.

(*k*) The initial depth of an uppermost layer, newly formed by the process discussed in (*g*), is determined by stipulating the following. The heat content of the new layer equals that of the thermal boundary layer ahead of the advancing front. The salt content equals that supplied by the basic salinity gradient, $d\bar{S}/dz$, over the new layer depth. The density step across the top of the layer (the new advancing front) is zero. Assumptions (*h*)–(*k*) are all made with an eye on the experimental results and their validity is discussed in § 5.4.

From these assumptions, we now turn to the mathematical model they imply. At any time let there be N layers with temperatures T_r, salinities S_r and depths h_r, where $r = 1, 2, \ldots, N$ and $r = 1$ is the lowermost layer. Let ϕ_r and ψ_r represent the heat and salt fluxes, specified according to (3.1) and (3.2), through interface r, which separates layer $r+1$ from layer r. Then conservation of heat and salt imply

$$h_1 \frac{dT_1}{dt} = 1 - \phi_1, \quad h_1 \frac{dS_1}{dt} = -\psi_1, \tag{3.3a,b}$$

$$\left.\begin{aligned} h_r \frac{dT_r}{dt} &= \phi_{r-1} - \phi_r \\ h_r \frac{dS_r}{dt} &= \psi_{r-1} - \psi_r \end{aligned}\right\} \quad r = 2, 3, \ldots, N-1, \tag{3.4a,b}$$

$$\frac{d}{dt}(h_N T_N) = \phi_{N-1}, \tag{3.5a}$$

$$\frac{d}{dt}(h_N S_N) = \psi_{N-1} - 2d_N(t)\frac{dh_N}{dt} \tag{3.5b}$$

and

$$T_N - S_N - 2d_N = 0, \tag{3.5c}$$

where

$$d_N(t) = \sum_1^N h_r \tag{3.6}$$

and (3.5*c*) follows from assumption (*e*).

The non-dimensional temperature profile $\theta(z,t)$ ahead of the advancing front satisfies

$$\frac{\partial\theta}{\partial t} = Q\frac{\partial^2\theta}{\partial z^2}, \tag{3.7}$$

$$\theta(z, t_N^0) = 0, \tag{3.8a}$$

$$\theta[d_N(t), t] = T_N(t), \tag{3.8b}$$

$$\theta(z,t) \to 0 \quad (z \to \infty), \tag{3.8c}$$

where t_N^0 is the time of initiation of the last advancing front.

Equations (3.3)–(3.8) are integrated forward in time until t_{N+1}^0, when the thermal boundary layer length scale

$$\delta = (2/T_N)\int_{d_N}^{\infty}\theta(z,t)\,dz \tag{3.9}$$

satisfies condition (2.9), that is

$$R = [T_N\delta^3 - 2\sigma(\sigma+1)^{-1}\delta^4]/(Q^2\sigma) = R_c. \tag{3.10}$$

At that time, layer $N+1$ forms with T_{N+1}, S_{N+1} and h_{N+1} initially determined as outlined in assumption (k). This implies that

$$T_{N+1}h_{N+1} = \int_{d_N}^{\infty}\theta(z, t_{N+1}^0)\,dz = \gamma_{N+1}, \text{ say}, \tag{3.11a}$$

$$S_{N+1}h_{N+1} = d_N^2(t_{N+1}^0) - [d_N(t_{N+1}^0) + h_{N+1}]^2, \tag{3.11b}$$

$$T_{N+1} - S_{N+1} - 2[d_N(t_{N+1}^0) + h_{N+1}] = 0. \tag{3.11c}$$

The solution of (3.11) is

$$h_{N+1} = T_{N+1} = \gamma_{N+1}^{1/2}, \tag{3.12), (3.13}$$

$$S_{N+1} = -[2d_N(t_{N+1}^0) + \gamma_{N+1}^{1/2}]. \tag{3.14}$$

As implied by assumption (j), if at any time $T_{i+1} - T_i = S_{i+1} - S_i$ for $i = 1, 2, \ldots, N-1$, layers i and $i+1$ merge to form a new layer i with temperature

$$(h_iT_i + h_{i+1}T_{i+1})/(h_i + h_{i+1}),$$

salinity

$$(h_iS_i + h_{i+1}S_{i+1})/(h_i + h_{i+1}),$$

and depth

$$h_i + h_{i+1}.$$

The system of equations (3.3)–(3.14) were solved numerically. Equations (3.3)–(3.5) were solved using a standard Runge–Kutta–Gill fourth-order method. Equations (3.7) and (3.8) were first transformed by introducing the new independent variable

$$x = z - d_N(t)$$

and then the resulting partial differential equation was represented by a space-centred finite difference array using the Crank–Nicolson implicit scheme (Smith 1965). This array was then solved by Gaussian elimination. The program was tested by comparing the results with particular calculations performed by hand. Accuracy and stability of the numerical algorithms were achieved by varying the time step and space step until suitable values were obtained.

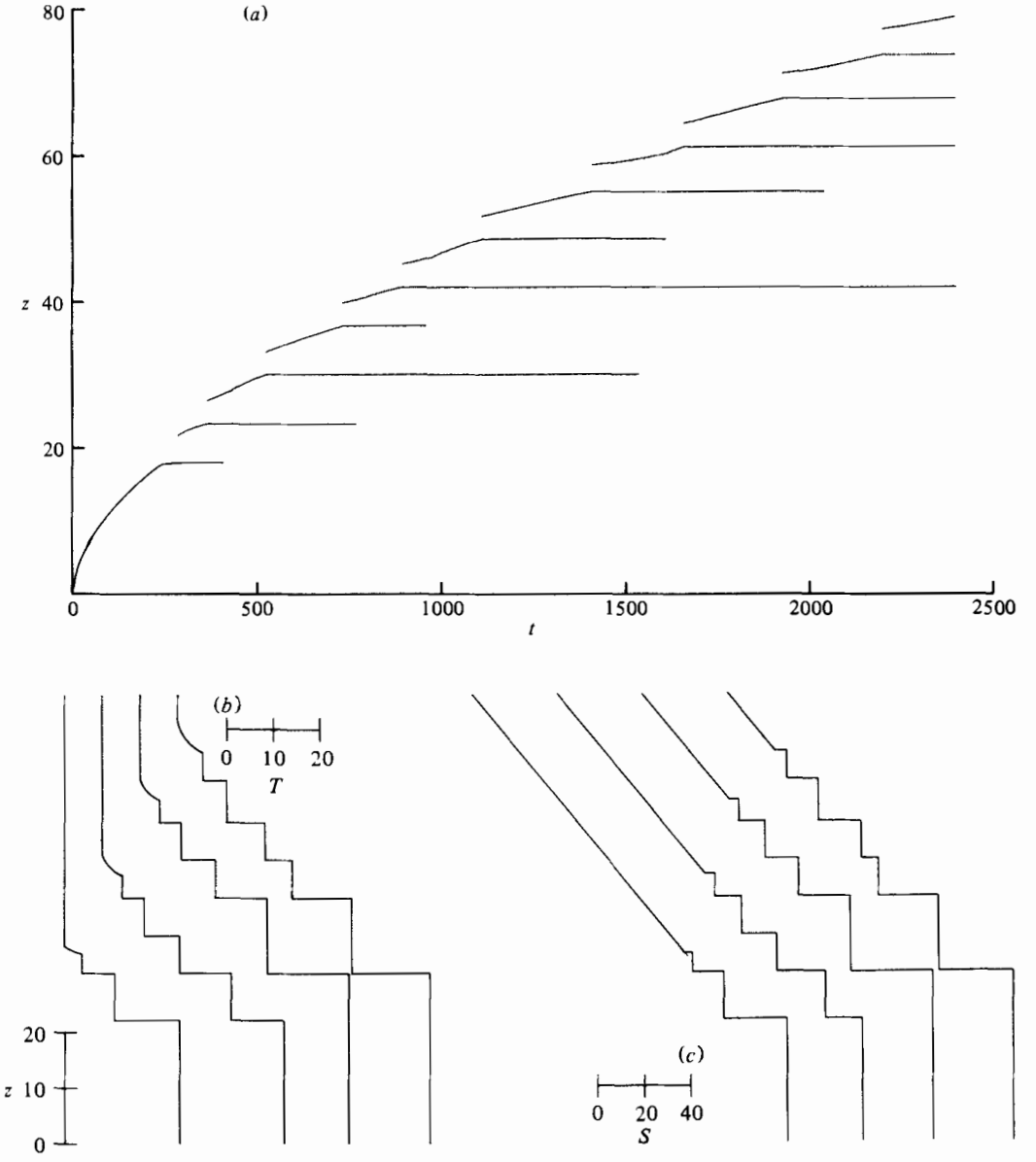

FIGURE 1. (*a*) The positions of the interfaces as functions of time for $Q = 0{\cdot}03$ and a constant coefficient of expansion. (*b*) The temperature profiles under the same conditions at $t = 600$, 1200, 800, 2400. The zero temperature axis of each successive profile has been offset to the right. (*c*) The salinity profiles for the same conditions and times as used for the temperature profiles. The salinity axis of each successive profile has also been offset to the right.

A typical result is shown in figure 1. The first layer grows as $t^{\frac{1}{2}}$ from zero thickness to its final value, at which time the second layer is initiated. The second layer's increase in thickness from its initial value is considerably less than that of the first layer as is the corresponding increase in the depth of subsequent layers. The height of initiation of the uppermost layer increases approximately like the square root of

time, as will be discussed further below. The temperature of each layer increases with time except at the instant when the layer is merging with the one above it. Analogously, the salinity of each layer decreases with time except when the layer is merging with the one below it. The stability ratio, $R_\rho = \Delta S/\Delta T$, of each interface generally decreases steadily from its initial value to 1·0, whereupon the two adjoining layers merge. However, abrupt increases or decreases in R_ρ also occur when either of the two neighbouring interfaces disappears. Ahead of the advancing front the temperature profile gradually increases in magnitude by conduction until it becomes unstable and a new layer is formed.

The system does *not* reach a state in which the final thickness of each new layer is exactly the same; the thicknesses become comparable, but not equal. Thus an exact steady-state envelope of advancing layers is not achieved.

The quantitative results of the calculation depend on a number of parameters, which include R_c, $\sigma/(\sigma+1)$ and the principal one, Q. The value of R_c is determined by equating the experimental measurement of the final thickness of the first layer to the theoretical value of h_1 as expressed by (2.11). As discussed in § 6 this procedure leads to $R_c = 10000$. Increasing R_c retards the breakdown of the boundary layer ahead of the advancing front and thus leads to thicker layers. However, as indicated in (2.11) the dependence of the height of the first layer on R_c is rather weak and the dependence of the thickness of subsequent layers on R_c is even weaker. Decreasing R_c leads to thinner layers.

The value of $\sigma/(\sigma+1)$ was set at 0·875, its value for water at room temperature. Increasing the value of $\sigma/(\sigma+1)$ retards the development of the layers and hence slightly decreases their number. However, the height of penetration of the series of layers is relatively independent of $\sigma/(\sigma+1)$. If $\sigma/(\sigma+1)$ is set to zero, the model produces a series of layers which are much thinner and more numerous than those observed in the experiments.

As explained previously, the only external parameter is Q. Decreasing Q increases the time at which any particular layer is initiated, as indicated by (2.8) and (2.11) for the particular case of the second layer. This increase occurs because decreasing Q reduces the effective diffusion coefficient ahead of the advancing front (see (3.7)), and the time for the stability criterion (3.10) to be attained is hence increased. The thickness of the layers is diminished by decreasing Q because of the smaller length scale associated with the boundary layer ahead of the advancing front. Finally, with decreasing Q the interfaces form with a reduced stability ratio and hence merging takes place more rapidly.

Despite these variations with Q, the height of the advancing front z_f is rather insensitive to Q and is well represented by

$$z_f = 1{\cdot}7t^{\frac{1}{2}}. \tag{3.15}$$

The data, both theoretical and experimental, supporting this conclusion appear in figures 18 and 19 and are discussed fully in §§ 6.4 and 7.

The main difference between the numerical model as so far presented and the experiments to be discussed in the following sections is the assumption that the coefficient of thermal expansion is constant. A variable coefficient, dependent on the temperature, of the form $\alpha_0\alpha(T)$ can be incorporated without too much difficulty. The changes required are minimized if it is assumed, as we shall, that α_0 is the

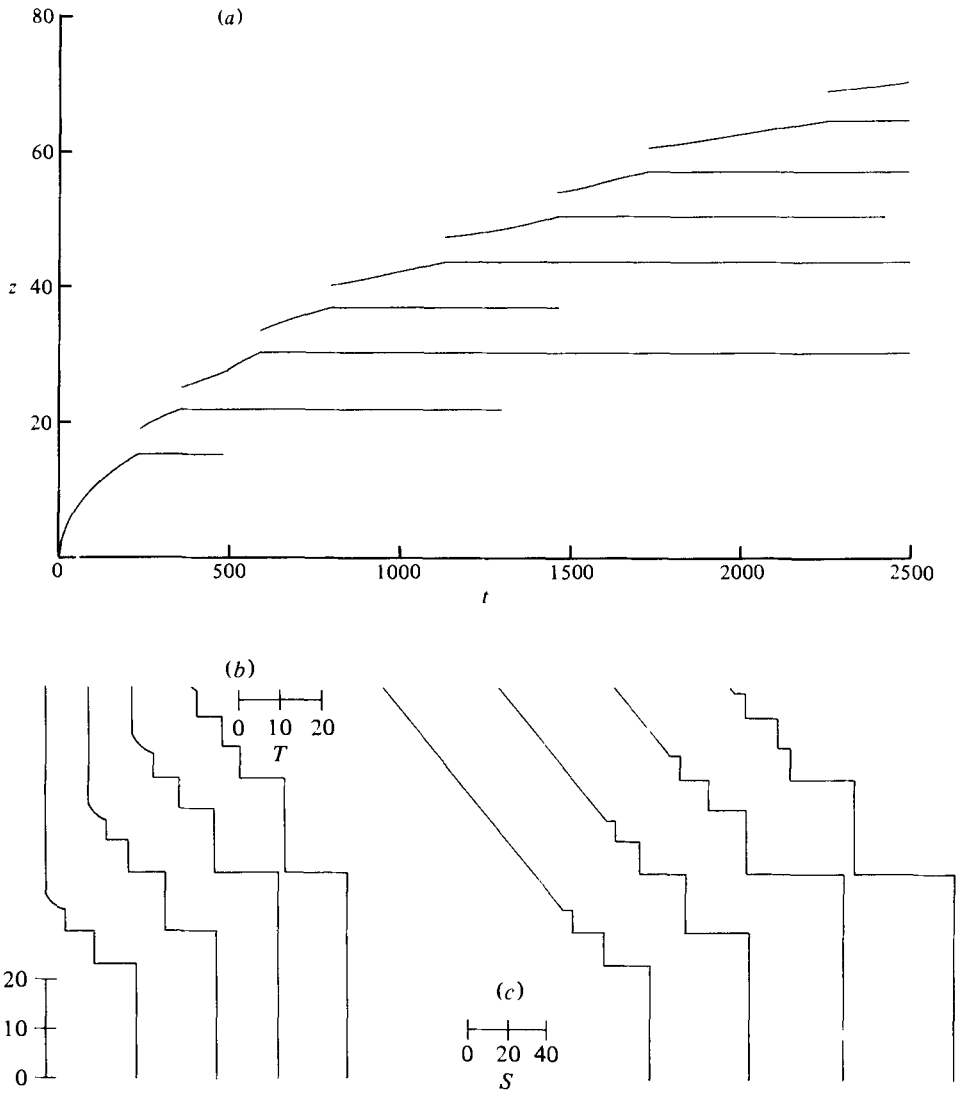

FIGURE 2. The positions of the interfaces and the temperature and salinity profiles as in figure 1 except that the variation in the coefficient of expansion has been included in the calculation as outlined in (3.16) and (3.17) with $H_* = 0{\cdot}0078$ cm^2 s^{-3} and $S_* = 0{\cdot}167$ s^{-2}.

coefficient of thermal expansion at a reference temperature well ahead of the advancing front and that in the thermal boundary layer attached to the advancing front $\alpha(T)$ differs from unity by an insignificant amount. The only changes then required are that (3.1) and (3.2) be replaced by

$$\phi = 0{\cdot}32(Q/\sigma)^{\frac{1}{3}}[\alpha(T)]^{7/3}\Delta T^{10/3}\Delta S^{-2}, \tag{3.16}$$

$$\psi = (1{\cdot}85\text{–}0{\cdot}85R_\rho)\alpha(T)\phi \quad (2 \leqslant R_\rho), \tag{3.17a}$$

$$= 0{\cdot}15\alpha(T)\phi \qquad (1 \leqslant R_\rho \leqslant 2). \tag{3.17b}$$

The linear relationship

$$\alpha = 1 + 0{\cdot}06\hat{T}, \tag{3.18a}$$

$$= 1 - 0{\cdot}06(\alpha_0 g)^{-1} H_*^{\frac{1}{2}} S_*^{\frac{1}{2}} T, \tag{3.18b}$$

which is appropriate for α throughout the temperature range covered by the experiments, leads to the results presented in figure 2. The effects of such a temperature-dependent coefficient of expansion are seen to be rather weak. The series of layers penetrates the water column somewhat more rapidly; for $Q = 0{\cdot}03$ ($H_* = 0{\cdot}0078$ cm^2 s^{-3}, $S_* = 0{\cdot}167$ s^{-2}), the value used in the preparation of figures 1 and 2, the difference is approximately 10 %. The lifetime of a particular layer is shorter and the merging of intermediate layers is rather more frequent. The number of layers present at any particular time is generally unaltered. Despite these differences being rather small, many of the features of the experimental results agreed better with the model incorporating a temperature-dependent expansion coefficient and this effect was therefore included. It should be noted, however, that incorporation of this non-Boussinesq term requires the specification of H_* and S_* separately.

A few numerical results were obtained with the break in the salt flux relationship, (3.2), at a value of R_ρ other than 2. There is some experimental doubt about the exact value of this break point (Crapper 1975; Marmorino & Caldwell 1976) and a more general relationship is

$$\psi = [1 - 0{\cdot}85(R_\rho - 1)/(R_\rho^* - 1)]\,\phi \quad (R_\rho^* \leqslant R_\rho) \tag{3.19a}$$

$$= 0{\cdot}15\phi \qquad (1 \leqslant R_\rho \leqslant R_\rho^*). \tag{3.19b}$$

The gross features of the resulting output were not much affected by a variation of R_ρ^* between 1·75 and 2·5. This will be discussed further in § 6.2 when the theoretical output is compared with the experimental results.

4. The experiments

The experiments were carried out in a modified version of Turner's original tank. The tank is a circular Perspex cylinder, 29 cm in diameter with a working depth of approximately 25 cm. For a few experiments an additional section of the same diameter was joined onto the tank to give a working depth of 85 cm. Heat was supplied through the base of the tank, a 6 mm thick aluminium plate, by an array of heater wires strung in an air space 5 cm deep. The heating was fairly uniform over the base of the tank. In order to try to improve the uniformity of the heating, in some experiments a thin sheet of asbestos was attached to the underside of the base plate, thereby providing a high thermal resistance. No appreciable difference in the motions produced in the tank was observed.

Salt was dissolved in degassed, distilled water and the solution allowed to stand until it had reached room temperature ($\sim$ 17 °C). A constant salinity gradient was produced by using the familiar 'double-bucket' method of Oster (1965) and by filling the tank through a freely floating sponge to inhibit vertical mixing. The magnitude of the density gradient was checked by withdrawing 1 ml samples at various depths and measuring their refractive index. Once the tank was filled, any necessary measuring probes were placed in position and the tank was insulated by surrounding it with 5 cm thick blown polystyrene. The heating was then begun with the rate of heating

controlled by a rheostat on the supply voltage to the heater wires. A sketch of the apparatus appears as figure 2 in Turner (1968).

In an attempt to maintain a constant heat flux during each experiment the supply voltage was initially set quite high and then gradually reduced to a constant value. The reductions had been predetermined on a trial-and-error basis to provide as constant a flux as possible, the flux being computed from the amount of heat in the tank as calculated from measured vertical temperature profiles. Typical plots of the heat content as a function of time are presented in figure 3, from which it is evident that after an initial adjustment period of approximately 15 min the flux is constant to within the scatter of the data. Since each experiment lasted at least 1 h, and most continued for considerably longer periods, the constancy of the heat flux appears to us to be satisfactory.

The heat flux H varied between 10^{-2} and 10^{-1} cal cm^{-2} s^{-1} and the proportional density gradient $\rho^{-1}d\rho/dz$ varied between -10^{-4} and -10^{-3} cm^{-1}. Resulting values of Q varied between 0·01 and 0·20. These values were to some extent dictated by the desire to have constant fluid properties during each experiment. The two fluid properties most seriously effected by the temperature variations are the Prandtl number and the coefficient of expansion. During the course of an experiment the temperature of the lower layer typically increased by approximately 10 °C. Thus the Prandtl number could vary between 7·5 at 17 °C and 5·5 at 30 °C. Potentially more serious is the variation in the coefficient of expansion between $-1{\cdot}8\times10^{-4}$/°C at 17 °C and $-3{\cdot}0\times10^{-4}$/°C at 30 °C. This implies that for the same heat flux H the dynamically important buoyancy flux $H_* = -\alpha gH/\bar{\rho}c$ can vary by almost a factor of two. The errors introduced by these effects are much greater than those due to the departure from linearity of the heat content as a function of time. They are discussed when the theoretical model and experiments are compared in § 6.

The measurements of temperature and salinity were made using thermocouples, thermistors and conductivity probes. These were all calibrated *in situ* and found to be drift-free within the accuracy of the calibrations over the period of each experiment. Temperature was measured to an accuracy of $\pm$ 0·05 °C and salinity to $\pm 1\times10^{-5}$ in density units, which is a proportional accuracy in salinity of 2%. The probes were either placed at fixed positions in the tank and monitored continuously or were traversed vertically using a motor-driven traverse. The length of the traverse was 17·5 cm and the probes were moved at around 0·4 cm s^{-1}, so that a typical traverse took somewhat less than a minute. The vertical resolution of all probes was estimated to be less than 0·2 cm at the operating speed. These measurements were all taken along a single vertical line, and although the horizontal position of the line was occasionally varied it is difficult to estimate the effects of spatial inhomogeneities in this way. Consequently a resistance-wire thermometer was used in one run. An enamelled copper wire was strung in a regular array across a circular Perspex support 15 cm in diameter, giving an average of the temperature along a horizontal path of 150 cm. This device was also traversed vertically and the results compared favourably with the output from the single probes.

Visual observations of the flow were made using time-exposed stills and cine films of aluminium powder suspended in the fluid. Shadowgraph observations were also made and these were used in the tall version of the tank to measure the layer depths. When quantitative measurements were made in this way the thermal insulation was

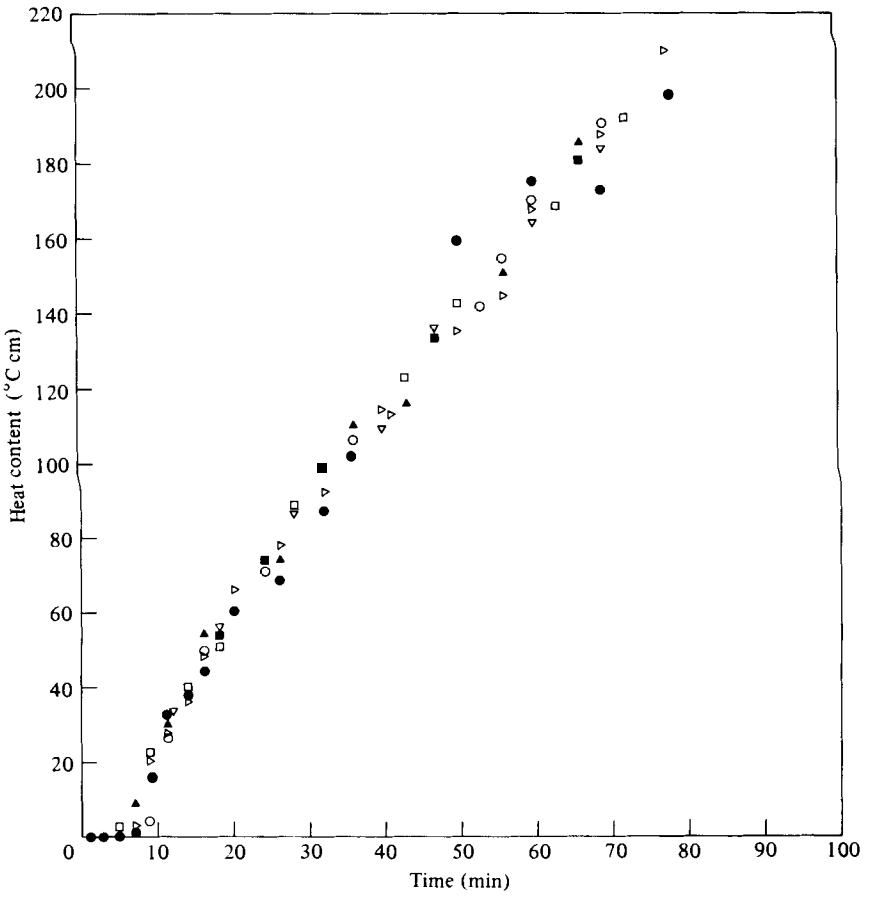

FIGURE 3. The heat content per unit area (°C cm) determined from the temperature depth profiles plotted against the time from the onset of heating. The results of seven experiments at the same external parameter settings are shown, each experiment being denoted by a different symbol.

removed just long enough for the layer depths to be recorded. Usually this process took about 1 min and was performed at most once every 15 min. We believe that this occasional removal of the insulation did not cause significant errors. For one set of parameters, a direct comparison was made with an experiment in the short tank when the insulation was not removed. No significant difference was found.

5. Experimental results

5.1. *Qualitative shadowgraph observations*

We begin the presentation of the experimental results with a discussion of some of the qualitative features of the flow. Depicted in figure 4 (plates 1–4) are shadowgraph views of a series of evolving layers. The layers are clearly visible and the production of new interfaces at the top and the loss of interfaces from the bottom with increasing time is evident. From pictures such as these and from time-lapse cine films a number of features are revealed. The most important is that the lowermost layer is deeper

than all of the others which are fairly similar in scale. The interfaces separating these layers, although horizontal on average, are buffeted by the turbulent convective motions in the layers and oscillate about their mean position. They have finite thickness, which can be as large as about 20 % of the depth of an adjoining layer. Except for the first interface, whose motion is discussed in § 6.1, and the advancing front, there is little mean vertical migration of individual interfaces. Some of the intermediate interfaces in the experiments in the tall tank, having occupied the same mean depth for several hours then migrated vertically over a period of 30 min to coalesce with an adjoining interface. See, for example, the merging of the central of the three somewhat diffuse interfaces (between the third and fourth layers from the bottom) that occurs from 0945 to 1030 on figure 4. Such occurrences were rare, though they have been observed in other experiments (Linden 1976), and we have as yet no explanation for them. We did note, however, that this type of merging tended to occur more frequently in the latter stages of the experiment. We will comment on this observation in § 6.3.

The production of a new layer at the top of the system is caused by individual convective elements which rise from the existing layer and ascend into the stably stratified region above. These motions are made visible by a 'cap' characteristic of such penetrative elements. An individual element is observed to rise a finite height and then slowly subside due to the stabilizing effect of the salinity gradient. In time the number of penetrating elements increases and they begin to mix up a new layer. Eventually a new well-mixed layer capped by an interface is formed. This typically occurs 5–10 min after the first rising element has been observed.

Most interfaces are destroyed at the bottom of the series of layers when the lowest layer joins with the one above. The lowest interface at 0203 on figure 4 is just about to disappear, and the large vertical excursions of the interface are characteristic of this stage. The merging takes place because the density of the lowest layer is continually decreasing owing mainly to the supply of heat from the bottom of the layer. Eventually its density becomes equal to that of the second layer and the two layers combine. Merging of intermediate layers also occurs, although much less frequently. We have already identified one case when the interface migrated vertically (0945 to 1030 on figure 4). An intermediate merging without interface migration seems to have occurred between 0449 and 0522.

5.2. *Aluminium powder observations*

Time exposures of aluminium particles suspended in the flow (figure 5, plates 5 and 6) also reveal the layered structure of the stratification. They indicate that the convective motions in the layers decrease in both magnitude and scale as the scale of the layers decreases. Also evident are the internal wave motions above the convective region excited by the convection impinging upon the stably stratified region. Time-lapse cine films revealed that the phase lines move downwards, indicating that energy, propagating in the direction of the group velocity vector, is being radiated away from the convective region by the waves. A similar occurrence, where internal waves were excited in a stably stratified fluid subject to mechanical agitation at the top, has been documented by Linden (1975).

From these photographs we can also dismiss the effect of side-wall heating as the cause for the layering. Turner was concerned about this effect in his experiments and

this was one reason why he only considered the formation of the first layer, where he was confident that side-wall heating was not important. From our visual observations, photographs and time-lapse cine films, we found no evidence that the layers developed laterally, spreading inwards from the outside. The convective motions had none of the organization typical of side-heated layers as seen, for example, in figure 5 of Chen, Briggs & Wirtz (1971). Quantitatively, Chen *et al.* found that the vertical scale of layers produced by side-wall heating of a stable salinity gradient is given by

$$\gamma\alpha_0\delta T/(\beta d\bar{S}/dz),$$

where δT is the temperature difference between the wall and ambient fluid and γ a numerical factor which varied between 0·6 and 1·0. In one of our experiments, we measured the difference between the mean temperature at the wall and that in the interior to be less than 0·2 °C. Taking $\beta d\bar{S}/dz = -2{\cdot}8\times10^{-4}$ cm^{-1}, $\alpha_0\delta T = -3{\cdot}6\times10^{-5}$, corresponding to $\delta T = 0{\cdot}2$ °C, and $\gamma = 1$, we obtain 0·13 cm as the maximum scale of layers produced by the horizontal temperature difference. The layer sizes actually observed were considerably larger, typically 1 cm, even at their inception. Thus from both qualitative and quantitative investigations we conclude that the layers were neither produced, nor had their depths set, by side-wall heating.

5.3. *Temperature and conductivity measurements*

The basic data obtainable by the probes are vertical temperature and conductivity profiles. Conductivity is a function of both temperature and salinity – the proportional influence of the two is roughly equal in density units, though the relationship between conductivity, temperature and salinity is not linear – and thus some qualitative indication of the salinity field is obtainable from the conductivity measurements. The clearest picture of the salinity field is obtained from that part of the conductivity profile where the temperature is uniform.

Typical profiles taken during the course of (different) experiments are shown in figures 6 and 7. During the experiments a profile was taken about every 2 min and recorded on an X, Y plotter. To produce figures 6 and 7 the original profiles have been traced and offset to the right. For clarity of presentation some of the profiles have been omitted, and so they are not evenly spaced in time. The profile on the extreme left of each figure represents the initial conditions of the experiments: uniform temperature and a constant salinity gradient.

The picture that emerges from the profiles is the same as that obtained from the visual observations. The heat introduced at the bottom of the tank produces a convecting layer there. Subsequently a second convecting layer forms, and then a third and so on. The layers are of fairly uniform properties and are separated by interfaces across which there are comparatively large changes in temperature and salinity. The profiles also indicate that the thickness of the interfaces, while small compared with the depth of the layers, is not extremely small, as has already been noted in the shadowgraph observations. In order to clarify the presentation we have drawn lines which mark the positions of the interfaces. These help to demonstrate the formation of new layers at the top of the system and the destruction of interfaces and merging of layers at the bottom. It should be noted, however, that the interpretations we have placed on the profiles by marking the interfaces are somewhat subjective. The two authors independently marked all the profiles and their interpretations occasionally

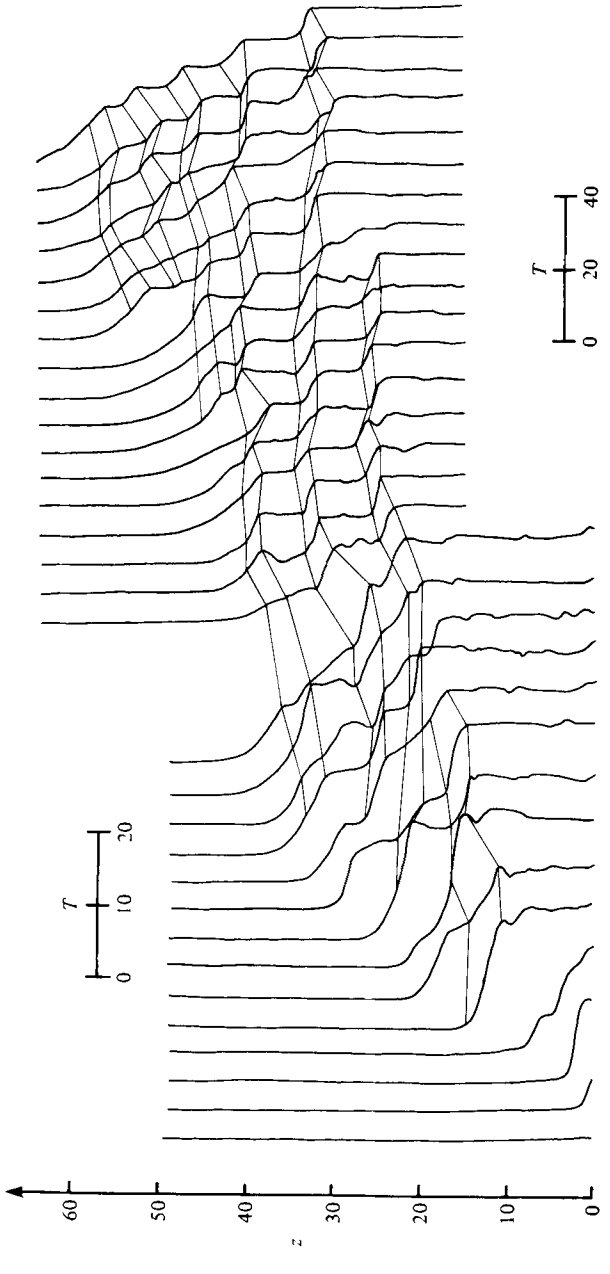

FIGURE 6. A set of temperature–depth profiles taken during the course of an experiment with $Q = 0{\cdot}03$. Each successive profile is offset to the right. The time between profiles was approximately 60 non-dimensional units (i.e. 2–3 min). At $t = 980$ the probe was raised 5 cm as is indicated on the figure and the temperature scale was halved. It is reasonable to suppose the lowest layer remains well mixed after that time. The horizontal lines joining points marking the edges of the layers on successive profiles provide indications of the positions of the interfaces. The identification is a subjective one and as stated in the text is merely used for illustrative purposes.

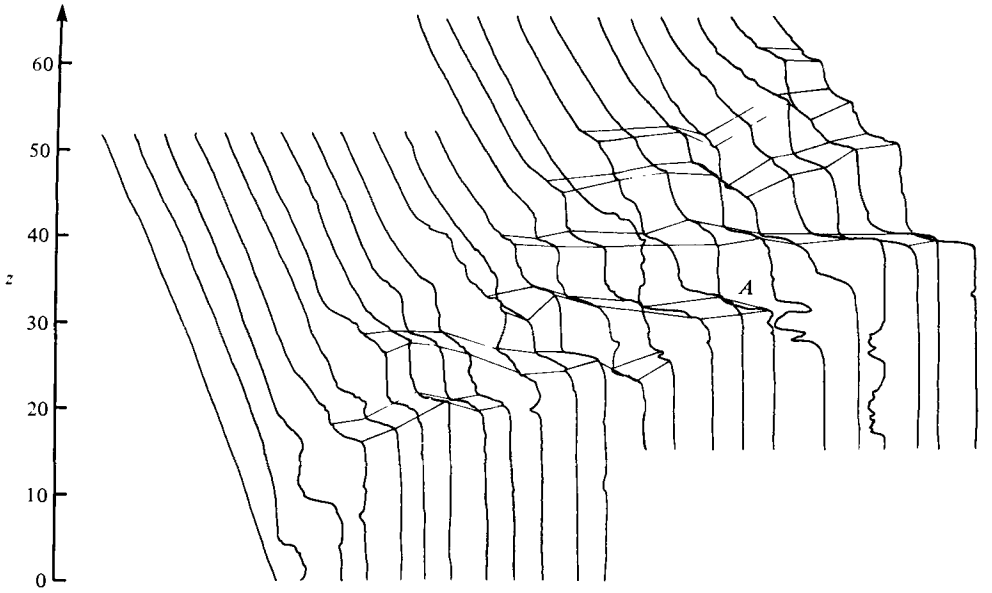

FIGURE 7. A set of conductivity–depth profiles for an experiment with $Q = 0{\cdot}03$. The markings on the figure are described in the caption to figure 6. The interface marked with the letter A is discussed on p. 450.

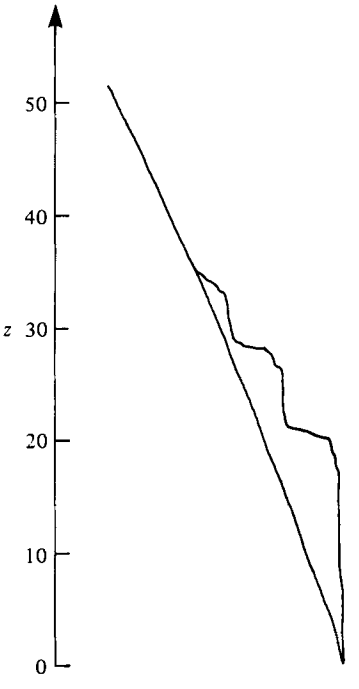

FIGURE 8. Two conductivity profiles taken before and 36 min after the start of an experiment. The profiles are plotted without adjustment and we note that above the convecting region the salinity gradient is unaltered from its original value.

differed. In each case it was impossible to decide on the correct marking, each author conceding that the other's interpretation seemed equally plausible! Also, it is not always possible to distinguish the same layers on successive traces and so sometimes it is impossible to avoid ambiguity. However, we do not place a great deal of stress on these interpretations for quantitative purposes and they are to be considered as mainly illustrative.

On figure 8 conductivity profiles taken before and about 36 min after the commencement of an experiment are plotted without adjustment. Above the three convecting layers the salinity gradient appears unaffected by the motions below. The internal waves, with typical vertical excursions of less than 0·25 cm, induce an isopycnal distortion too small to detect on the profiles.

5.4. *Experimental investigation of the theoretical assumptions*

It was immediately noticed on performing the experiments that even when operating conditions were the same there were significant variations in the profiles measured at the same times in different runs. Consequently, we decided that in order to make a meaningful comparison between the theoretical model and the experiments it was necessary to average the results over a number of experiments. Hence we carried out 10 experiments using the same initial salinity gradient and heating rate, and thus the same value of Q. The value of Q chosen was 0·03 ($H_* = 0{\cdot}0078$ cm^2 s^{-2}, $S_* = 0{\cdot}167$ s^{-2}) as this seemed to be a suitable value given the experimental tank and heating apparatus available and the fact that we wanted to restrict the fractional variation in fluid properties during the experiment to be small. From these 10 experiments we were able to make ensemble averages of the layer scales and temperatures with which to compare the calculations of the theoretical model.

We begin by considering the assumptions used in the model, in the order they are presented on p. 434.

(*a*) *One-dimensionality*. This assumption has two main ingredients. The first is that the formation of a new layer, resulting from the breakdown of the unstable boundary layer, takes place simultaneously over the whole horizontal plane. In practice, we only require that there be no persistent horizontal variations as would be caused, for example, by side-wall heating. As has already been mentioned, we found no evidence of such effects and so the treatment of the breakdown as a one-dimensional process can be regarded as satisfactory. The second ingredient concerns the nature of the layers once formed. Streak photographs (figure 5) indicate that there are small-scale motions with aspect ratios around unity within the layers, but on average the interfaces appear to be horizontal and the mean properties of the layers independent of horizontal position. Although we did not look in detail at horizontal variations in salinity and temperature, we infer the latter result from two independent sources. These were comparisons of the point probes (thermocouples and thermistors) with the resistance wire which gave a horizontal average of over 150 cm, and comparisons of vertical profiles taken at different horizontal positions. The mean properties of the layers measured in each case were in good agreement with one another.

(*b*) *Vertical uniformity within layers*. Both the profiles of temperature and conductivity indicate that layers, once formed, are well mixed in the vertical. Typical temperature gradients in the layers were of the order of 10^{-2} times those in the interfaces.

(*c*) *Neglect of heat transfer across the advancing front.* The experiments cannot directly examine the consequences of this assumption. However, calculation of the heat content ahead of the advancing front from the profiles presented in figures 6 and 7 confirms that it is typically very much less than the heat input at the bottom. From these figures it can also be deduced that the heat flux into the uppermost layer is typically an order of magnitude greater than the heat loss across the advancing front.

(*d*) *Diffusion of salt.* The diffusion of salt has been neglected when calculating the criterion for the breakdown of the advancing boundary layer. This implies that the original salinity gradient remains unchanged until the boundary layer becomes unstable. Since heat diffuses about 100 times more rapidly than salt, diffusion of salt will only affect the inner tenth of the thermal boundary layer. The salt boundary layer would therefore typically be about 0·2 cm thick, which is probably at the limit of the resolution of the conductivity probe. Within this limitation, measurements of salinity across the thermal boundary layer indicate that the original salinity gradient is unaltered until the interface breaks down.

(*e*) *Zero density step across advancing front.* The model assumes that there is no density discontinuity at the top of the growing layer. Figure 9 shows a comparison of the conductivity and temperature profiles measured simultaneously by two probes with approximately 0·5 cm horizontal separation. It is sometimes difficult to identify the top of the growing layer (in this instance the first layer) but we take it to be marked by the large conductivity gradient at the top of the mixed region (at $z = 17$). From the conductivity and temperature of the mixed layer we calculate its salinity and find that the value is entirely consistent with that obtained by supposing that salt is conserved in the layer and the initial salinity gradient is mixed over the layer. The change in density across the top of the layer due to salt is marked ΔS on figure 9. We then calculate how large ΔT would need to be in order to satisfy the condition of zero density difference: $\Delta T = \Delta S$. The result is shown by the right-hand vertical line on figure 9. The error bars on either side of the line result from taking extreme values of α, associated with the ambient temperature and the temperature of the lower layer. The vertical line denotes the mean value of these two extremes. The assumption of zero density difference is clearly very reasonable since the net density step is at most 10% of either ΔS or ΔT. For the second and successive layers the validity of this approximation is more difficult to check as the temperature and salinity steps across the advancing front are smaller than for the first layer. However, where it is possible to identify the front, it appears that the assumption that $\Delta T = \Delta S$ is justified.

(*f*) *Critical Rayleigh number.* The criterion for the breakdown of the unstable boundary layer ahead of the advancing front is that

$$R = R_T - \frac{\sigma}{\sigma+1} R_S$$

exceeds a critical value R_c. From his calculations for the first layer, Turner (1968) found that $R_S \ll R_T$ and that R_c is of order 10^4. Consequently he neglected the salinity gradient and equated R with R_T. From the temperature profiles we are able to establish that while R_S does not remain small compared to R_T for the later layers, the Rayleigh number immediately prior to the formation of a new layer is of order 10^4, in agreement with Turner's result. We can see how the relative importance of R_S increases as the series of layers develops. The heat flux into the uppermost layer

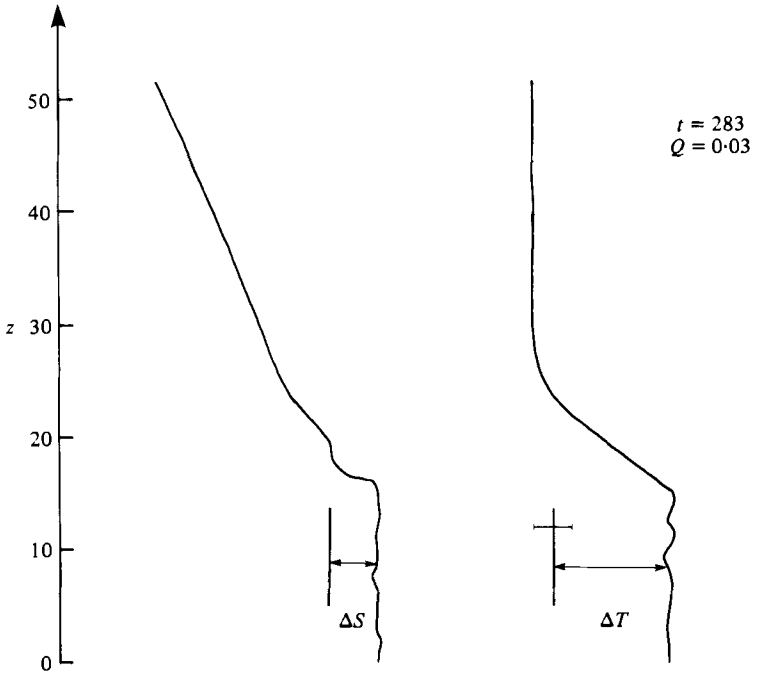

FIGURE 9. Conductivity and temperature profiles measured by two probes with 0·5 cm horizontal separation. The salinity step across the top of the first layer is indicated by ΔS. The equivalent temperature step given by $\Delta T = \Delta S$ is also shown. The value of α is taken to be that appropriate to the mean temperature, with the excursions shown resulting from α taking its extreme values appropriate to the ambient or layer temperature.

decreases due to the increasing number of lower layers. This reduced heat flux decreases the temperature excess of the uppermost layer with respect to previous ones. Consequently, the (non-dimensional) length scale of the boundary layer, ahead of the advancing front when $R = R_c$, increases. But

$$R_S/R_T = 2\delta/T_N$$

[cf. equation (3.10)], and thus both the increasing value of δ and the decreasing value of T_N increase the importance of R_S with respect to R_T.

(*g*) *Instantaneous response at breakdown.* Having established from the profiles that $R_c \sim 10^4$ prior to the formation of a new layer, we now turn to the events immediately following the fulfilment of this condition. The assumption is that the new layer forms instantaneously and that the growth of what was previously the upper layer ceases at this time. An examination of the profiles reveals that the formation of the new layer is not instantaneous, as it is not always visible in successive profiles (see, for example, profiles in figure 6). The formation of an established convecting layer can take 5–10 min after what appear to be the initial signs of breakdown of the unstable boundary layer. The assumption that the preceding layer stops growing at this point is also only approximate. It appears to be least valid for the first layer, which can grow by as much as 20% of its final depth after the appearance of the second layer.

For later layers, whose change in depth is much smaller than that of the first layer, the assumption is more accurate. Typically, for these layers the growth after the next layer has formed adds less than 5% of their final depths. Both of these processes, the delay in mixing a new layer and the continued growth of the preceding one, result in a lag between the time at which the boundary layer becomes unstable to infinitesimal disturbances and the time at which a new layer is established. This time lag is parameterized through the critical Rayleigh number R_c of the model. It has already been noted that R_c is an order of magnitude larger than we should expect on the basis of linear stability theory. Since the Rayleigh number for the boundary layer increases with time, the large value of R_c allows the model to adjust to the time lag of the experiments.

(*h*) *Constant layer depths.* The assumption that all the layer depths apart from the uppermost one are constant in time is confirmed by almost all our observations: see, for example, figures 6, 7 and 16. The exceptions to this rule occur when an interface migrates vertically until it joins with an adjacent one. As noted above, this is an infrequent occurrence and is neglected in the numerical model.

(*i*) *Heat and salt transfer relations.* The explicit testing of these relationships, equations (3.1) and (3.2), during a series of experiments would be a large, and in the authors' opinion unwarranted, task. The relationships have been well documented by previous experiments (Turner 1965; Crapper 1975), and shown to be applicable to large-scale situations (Huppert & Turner 1972). The degree of agreement between our theoretical model and the current experiments goes some way to supplying an additional confirmation of their validity.

(*j*) *Layer merging.* The breakdown of intermediate interfaces and the merging of the lower layers is assumed in the model to occur when the density of a given layer becomes equal to an adjacent one. The model also assumes that during the merging process there is no mean vertical migration of the intervening interface. Previous experiments (Linden 1976) on diffusive layers in salt–sugar stratification documented two kinds of layer merging: one in which the interface maintains its mean vertical position and progressively becomes more distorted and eventually breaks down, and the other in which the interface remains coherent, migrating vertically until it reaches another one. It is the first of these mechanisms that is incorporated into the model and is in agreement with what is most frequently observed. For example, in the case of the breakdown of the interface marked with an A on figure 7, the density ratio across each interface, R_ρ ($= \Delta S/\Delta T$) was calculated for the four profiles immediately prior to the merging of the layers. R_ρ was found to decrease monotonically taking the values 1·7, 1·65, 1·6 and 1·5. Measurements indicate that the heat and salt content of the layer formed by the destruction of this interface equalled that in the two layers immediately prior to breakdown.

Merging produced by the mean vertical migration of an interface is not yet understood and is not included in our model. Fortunately, this form of merging occurs only occasionally in the experiments and so the errors introduced by neglecting it are not large. This may be due to the parameter range we are considering in the present experiments, since for salt–sugar interfaces Linden found that interface migration was the more frequent mechanism by which layers merged.

(*k*) *The depth of newly formed layers.* It would be virtually impossible to test directly the assumptions that are employed to determine the depth of the uppermost

layer at its inception. However, the calculated and observed depths are comparable, which gives support to the assumptions employed.

6. Comparison of the experimental results with the model

6.1. *Calibration of the model*

The model has one adjustable parameter, the critical Rayleigh number R_c, which determines the breakdown of the unstable boundary layer at the front of the growing layer thereby producing a new layer. In order to determine the value of R_c, detailed comparisons between the model and the experiments were carried out at one value of Q.

In total, ten experiments were carried out with $Q = 0{\cdot}03$ and these different realizations were analysed to provide ensemble averages of the data. Each run was examined at five pre-set times during the development of the layers. Ensemble averages of the vertical profiles measured at each of these times were made, giving five mean profiles. Mean profiles were only calculated for temperature, as conductivity was not measured in every experiment. However, when measured, the number and depth of the layers obtained from conductivity measurements was the same as that obtained from the simultaneous temperature profiles, thus adding confidence to the realiability of the latter.

In order to calibrate the model only the depth of the first layer is needed. In § 2 we showed that the final depth of the first layer, h_1, for given Q and molecular properties depends only on R_c. Unfortunately, there is some ambiguity in the determination of h_1 from the profiles. As mentioned earlier a layer does not stop growing immediately the next layer is formed: this is particularly true of the first layer, which being closest to the heat source is the most vigorously convecting. Furthermore, $R_c \propto h_1^4$ and so a small error in h_1 leads to large uncertainties in R_c.

A lower limit on h_1 is obtained at the first evidence of an established second layer in the profiles. This procedure is somewhat subjective but reasonably consistent results were obtained using it. A difficulty arises from the fact that even after the formation of the second layer the first layer continues to grow, though considerably less rapidly, until it eventually merges with the one above. It is not always easy to tell from the profiles when this merging occurs. Consequently, an independent check was used. This is provided by measurements of temperature at a point inside the first layer as time increases. These measurements were obtained from the profiles and an example is displayed in figure 10. We note that the temperature of the layer increases as expected due to heating from below (which significantly exceeds the heat loss from the top). However, at $t \doteqdot 700$ the temperature decreases. This is due to mixing of the colder fluid down from above when the first layer merges with the second, as is confirmed by the profile. From plots such as these, we determine the time at which the first layer merges in each case and, consequently, its ultimate depth. It is also possible to identify subsequent mergings from plots such as these. A second merging occurs at $t \doteqdot 1100$. The results of the two procedures give $h_1 = 16{\cdot}1 \pm 1{\cdot}2$ (initial) and $h_1 = 19{\cdot}7 \pm 0{\cdot}8$ (ultimate). Thus the first layer grows by 21% (on average) from the time the second layer first appears until it merges with the second layer. It should be noted that this growth is only about twice the thickness of the interface at the top of the layer.

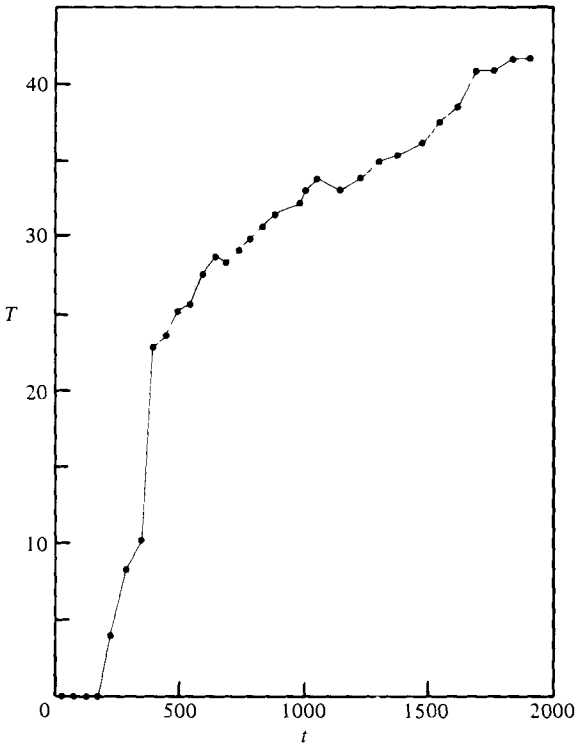

FIGURE 10. The temperature at a fixed depth (z = 15·3) plotted against time t. The temperature was determined from temperature–depth profiles such as are shown on figure 6, and each datum point corresponds to a different profile. The straight line segments are drawn in for illustrative purposes. Q = 0·03.

As the first layer is observed to grow more after the formation of the second layer than is typical for all the later layers, it is inappropriate to take its ultimate depth as the best determination of the R_c. Rather, we choose the mean of the two values given above, h_1 = 17·9, which implies that R_c = 10000. Taking the upper and lower values given above yields $R_c = 2{\cdot}2 \times 10^4$ and $0{\cdot}65 \times 10^4$ respectively. The two values of h_1 given above differ only by 1 cm (in dimensional units), showing how sensitive R_c is to the choice of h_1. Conversely, the depth of the layer is an insensitive function of R_c and so for the purpose of calibrating the model it is not essential to be very accurate in the determination of R_c.

6.2. *Detailed profiles in the small tank*

Having determined the value of R_c from the depth of the first layer, we are now in a position to compare the subsequent evolution predicted by the model with the experiments. This comparison is shown on figures 11, 12 and 13. Each of these figures shows an ensemble average temperature–depth profile determined as described above and the model results appropriate to the time these experimental profiles were obtained. Three examples have been chosen corresponding to profiles near the beginning, middle and end of the experiments in the small tank. The hatched area spans plus and minus one standard deviation from the mean of the experimental results. The

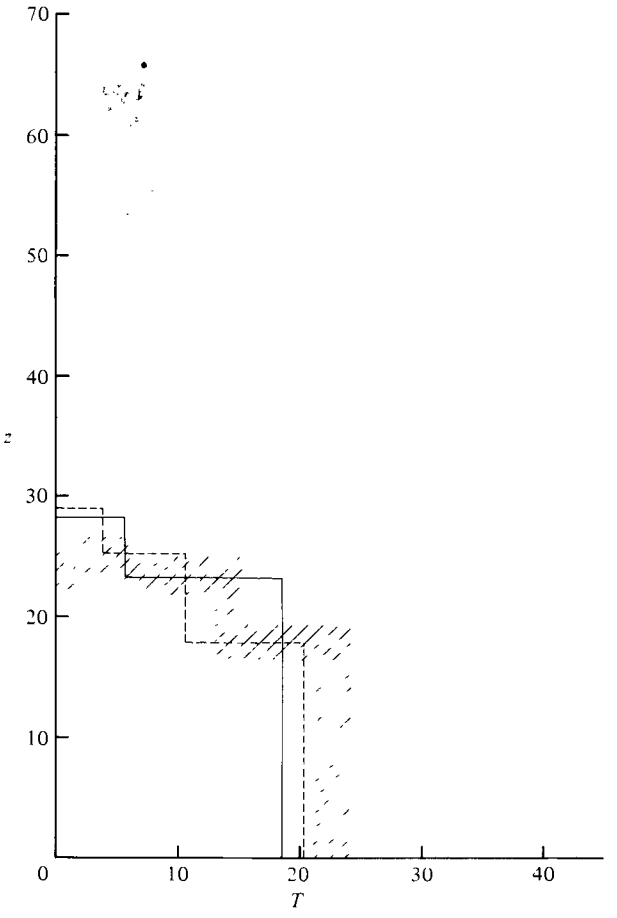

FIGURE 11. Comparison of the ensemble average temperature–depth profile obtained from the experiments with $Q = 0{\cdot}03$ with the results of the model at $t = 443$. The shaded area spans ± 1 S.D. from the mean of the experimental results. The solid line represents the model calculation for $R_c = 10000$ and $R_\rho^* = 2$. The broken line corresponds to $R_c = 10000$ but with $R_\rho^* = 1{\cdot}75$.

solid line represents the profiles obtained from the model using $R_c = 10000$. It should be noted that, in all these comparisons, the variation in α with temperature has been taken into account.

For the earliest profile ($t = 443$) we see that in the experiments there are two, and sometimes three, layers. The model calculations give two layers at this time. However, we note that the depth of the lowest layer is approximately 20 % greater in the model and its temperature is less. This is a result of the fact that just before this time the first and second layers had merged in the model calculation. Thus the depth of the lowest layer in the model is actually the sum of the first and second layers, which is in good agreement with the experiments.

For $t = 1227$, the depth and temperature of the lowest layer are in good agreement with the experiments. The lowest layer is considerably deeper than at $t = 443$ owing to successive merging of the bottom layers. It has also increased in temperature owing to the net gain of heat caused by the constant heat flux at $z = 0$. The detailed

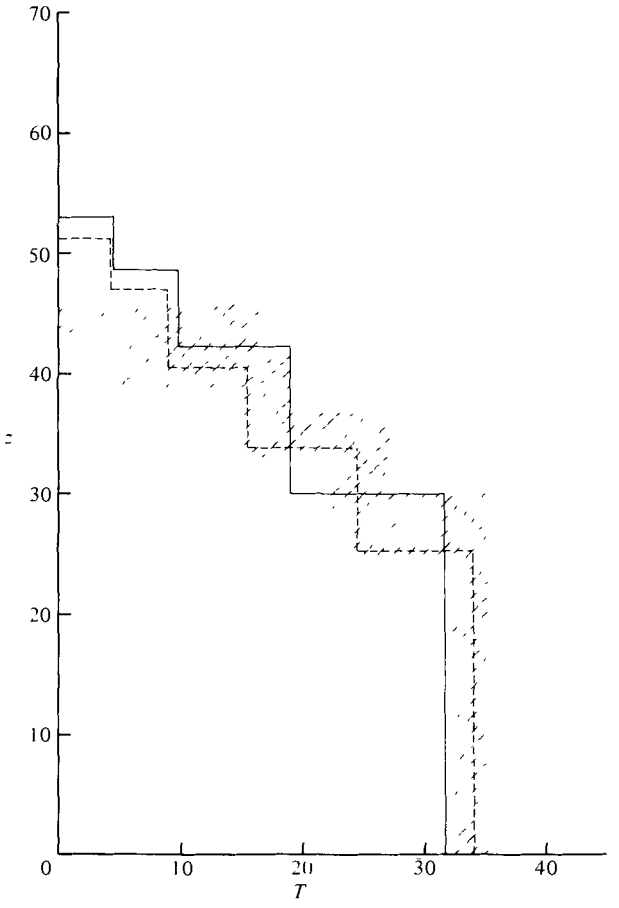

FIGURE 12. Comparison of the ensemble average temperature–depth profile obtained from the experiments with $Q = 0{\cdot}03$ with the results of the model at $t = 1227$. The details are described on the caption to figure 11.

agreement within the remainder of the profile is not as good. Although the model correctly predicts the number of layers, it overestimates the depth of the second layer. This is caused by the merging of two intermediate layers which is only rarely observed in the experiments. We also note that the total depth of fluid which has been formed into layers is overestimated by about 10 %.

The final profile taken at $t = 1916$ is shown on figure 13. As in the previous two cases, the model is in broad agreement with the observations, but differs in detail. Most notable is the fact that the lowest layer is much deeper in the model. As in the case for $t = 443$, this is because the lowest layer has merged more rapidly in the model than in the experiments. The model also continues to overestimate the total depth of layer formation. In this case, however, part of the cause may be the proximity of the (insulated and rigid) top of the tank which is at $z = 72$. Experiments in the deeper tank showed that this overall depth is predicted quite well by the model (see figure 19). It is also evident from figure 13 that the total heat content in the experiments is less than that in the model at this time. This is due to the decrease in the heat flux at later stages in the experiment, as depicted in figure 3.

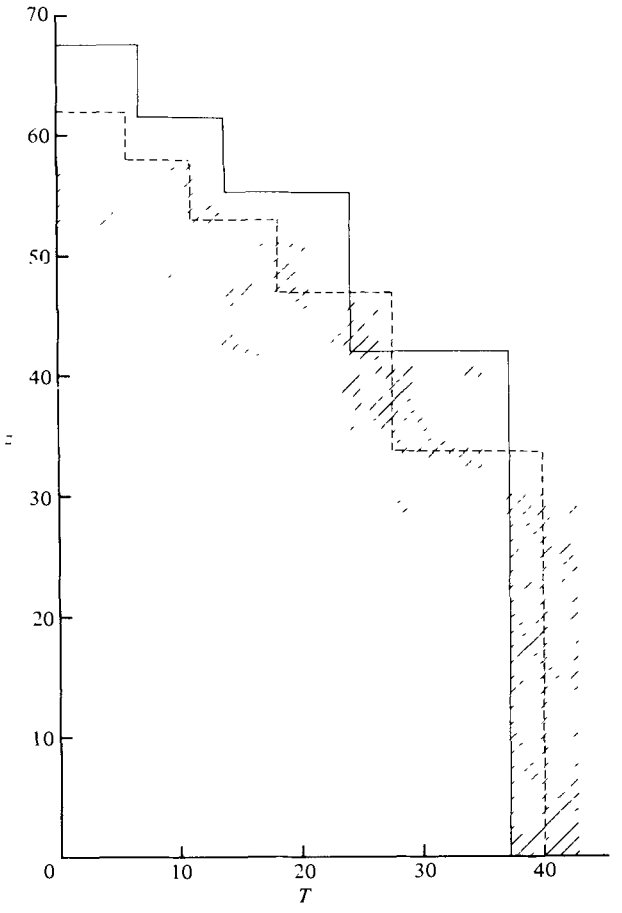

FIGURE 13. Comparison of the ensemble average temperature–depth profile obtained from the experiments with $Q = 0{\cdot}03$ with the results of the model at $t = 1916$. The details are described on the caption to figure 11.

In summary, the model gives broad agreement with the experiments but does show some differences of detail. These discrepancies appear to result from the fact that the model predicts that layer merging takes place more rapidly than is observed. There are a number of possible causes for this. It is possible that the procedure of assuming that the two layers mix instantaneously at $R_\rho = 1$ does not correctly model what happens in practice. Though we observed quite rapid breakdown of the interfaces, it is possible that this might begin with the interface still slightly stable ($R_\rho > 1$) due to the convective stirring in the layers.

Huppert (1971) has shown that a system of layers is stable provided the ratio of salt flux to heat flux across each interface is independent of ΔS and ΔT. Using the flux laws (3.2) taken from Turner's data, we see that this ratio is constant provided $R_\rho > 2$, and is variable for $1 < R_\rho < 2$. When a new layer is formed, both the experiments and the model show that R_ρ across the lower interface is some value greater than 2. As time proceeds R_ρ is observed to decrease. Eventually, for any interface $R_\rho = 1$ and the two adjacent layers merge. On the basis of Huppert's theory and also

from the model calculations, it is found that once $R_\rho < 2$ the rate of decrease in R_ρ becomes more rapid, soon leading to the breakdown of the interface. This suggests that it is possible to delay the layer mergings by decreasing the value, R_ρ^*, at which the flux ratio becomes variable. This was done by using (3.19*a*) and (3.19*b*).

It was found that, although the gross features of the profiles were not particularly sensitive to the value of R_ρ^*, the detailed structure was. This is revealed by the broken-line profiles shown on figures 11, 12 and 13, which are the model results for identical calculations to the above except that $R_\rho^* = 1{\cdot}75$ instead of 2·0. We see that in all cases this gives much better agreement with the experimental profiles, predicting quite accurately both the temperature and depth of the layers.

6.3. *Results from the deep tank*

The qualitative picture that emerges from these experiments is of a set of layers moving up the water column. New layers are produced at the top of the existing ones and old ones merge at the bottom to produce a deep-convecting region below. The question of whether this system could attain a kind of steady state with the production of new layers equalling the destruction by merging so that a fixed number of layers move up the column was raised by Turner (1968).

The behaviour of the system at large times was studied in the deep tank. Figure 14 shows a plot (on a logarithmic scale) of the depths of the top and bottom interfaces against time. After some initial irregularities, the data settle on to two parallel straight lines with slope $\frac{1}{2}$. Thus the total depth of convecting fluid and the depth of the lowest layer both increase like $t^{\frac{1}{2}}$. The number of layers is plotted against time in figure 15. This is a logarithmic plot and a line proportional to $t^{\frac{1}{2}}$ is drawn for comparison. Although these data are more scattered, we see that the number of layers also increases like $t^{\frac{1}{2}}$. Since the depth of the region occupied by the layers is proportional to $t^{\frac{1}{2}}$, this implies that all the layers, apart from the lowest layer, are roughly equal in size.

The uniformity in the layer size can be seen quite clearly on figure 16, which shows the details of the layering. In this example, the system was observed at discrete times during the experiment and the depths of the existing interfaces noted. Each observation gives the (t, z) co-ordinates of an interface, and a sequence of co-ordinates with fixed z as t increases indicates that an interface stays at that height for some interval of time. Figure 16 is obtained by drawing in lines of constant z between the data points. Due to the discrete sampling times, this is a slightly subjective process if z is not exactly constant, but it is possible to construct the life histories of the individual interfaces in this way. This figure reveals the same gross features as described above. The parabolic growth of the height of the top of the layers and of the depth of the lowest layer is clearly visible. It is also evident that the vertical scale of the layers is approximately constant.

Several other interesting features emerge. As the system evolves, the lifetimes of the individual interfaces tend to increase. Since the thickness of the set of layers (excluding the bottom) is proportional to $t^{\frac{1}{2}}$ and the upward velocity of the set is proportional to $t^{-\frac{1}{2}}$, the lifetime of an interface is proportional to t_N^0, the time at which it is formed. In the early stages of the experiment, layer merging takes place successively from the bottom. However, later on mergings are observed to occur between intermediate layers: see, for example, the two layers at $z \sim 200$ which merge

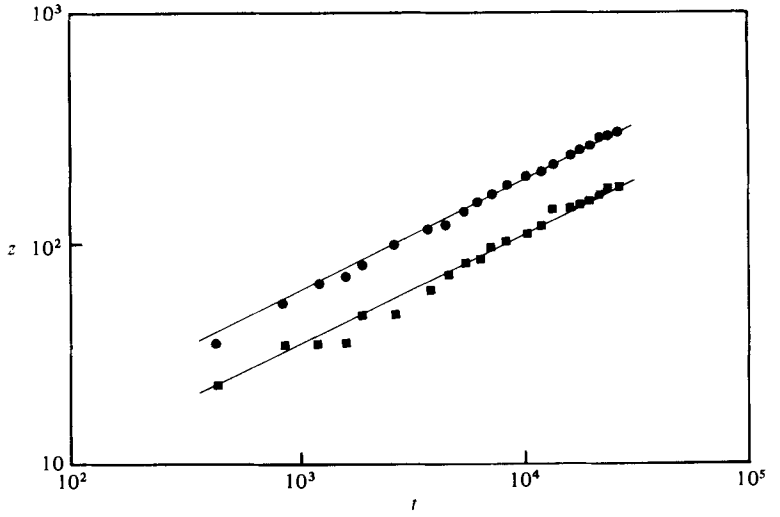

FIGURE 14. The depths of the uppermost and lowest interface determined from shadowgraph observations plotted against the elapsed time for $Q = 0{\cdot}047$ ($H_* = 0{\cdot}0078$ cm^2 s^{-3}, $S_* = 0{\cdot}256$ s^{-2}). The plot is logarithmic and the two straight lines have slope of $\frac{1}{2}$ and are positioned by eye.

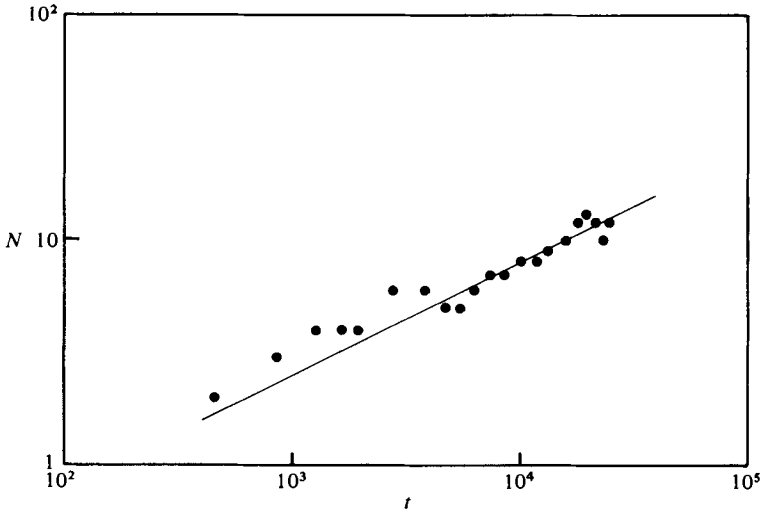

FIGURE 15. The number of layers N plotted against the elapsed time for $Q = 0{\cdot}047$. The plot is logarithmic and the straight line, positioned by eye, has slope $\frac{1}{2}$.

at $t = 20000$. In this case the two interfaces appear to approach each other in the final stages before coalescing to form a single interface at a depth midway between the original pair. Migration of an interface before it merges is also evident in the interface at $z = 230$ which has practically merged at the end of the measuring period. In contrast the interface at $z = 265$ appears to break down without any appreciable vertical migration in a manner similar to the interfaces at the bottom of the system.

Model calculations run over longer times have many features in common with those found in the deep tank experiments. Figure 17 presents the details of the evolving

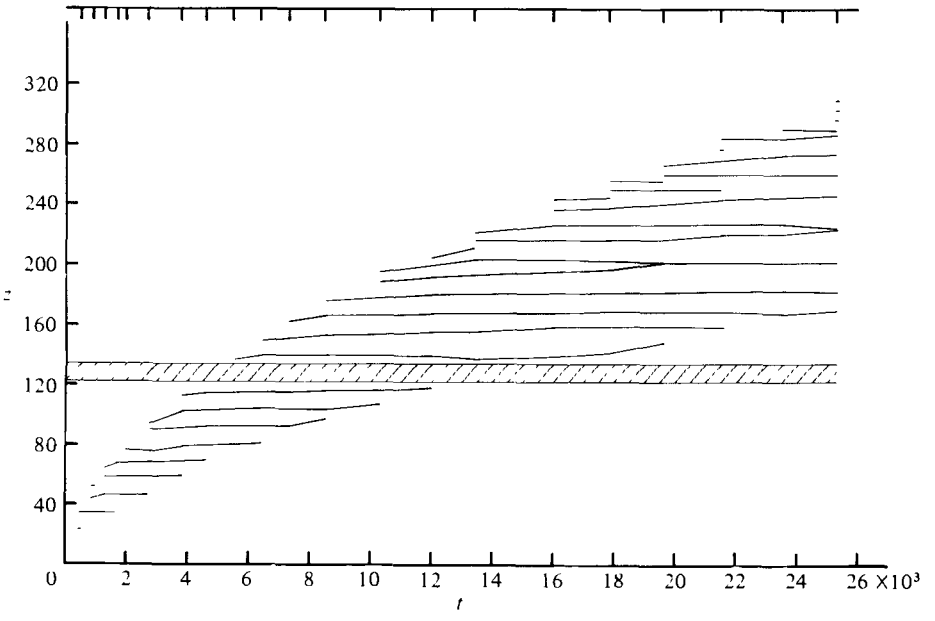

FIGURE 16. A life history of the convection (Q = 0·047). The system was observed by viewing the shadowgraph at the times indicated by the marks at the top of the figure. At each observation the depth of each interface was measured. This figure is constructed by drawing lines between each pair of data points where we were reasonably sure that an interface had existed between observations. Thus the solid lines represent the position of the interfaces from the time they were formed until they were destroyed by the merging of two layers. The hatched region represents the join between the walls of the small tank and the additional section visible on figure 4 (plates 1–4). No observations were possible over this region.

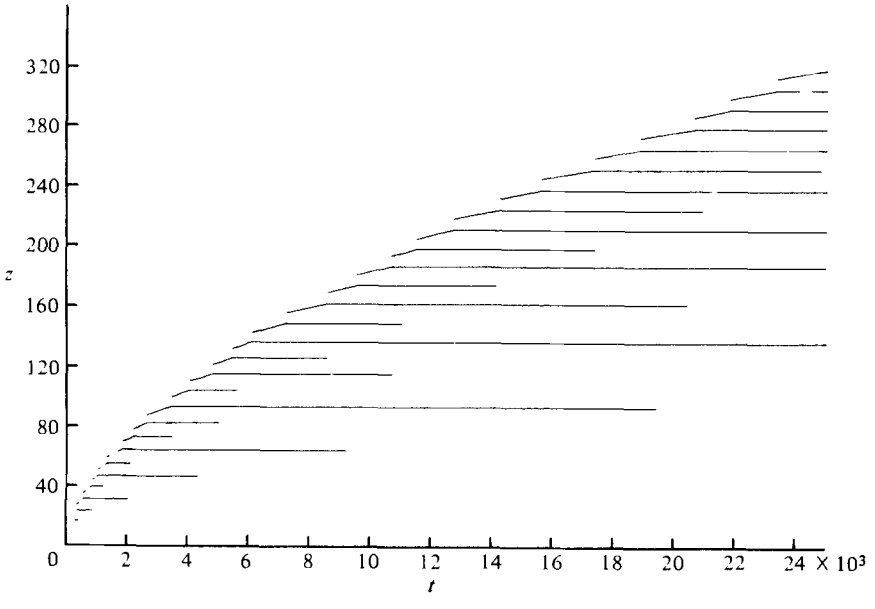

FIGURE 17. The results of the model calculations for the same parameters as in figure 16.

layer structure for the same parameters as the experiment which is described by figure 16. The agreement between the two is seen generally to be very good: the height of the convecting front increases in much the same way as in the experiment and the size and number of the layers are very similar. The major differences between the model and the experiments is that in the initial stages of the evolution the model predicts the existence of interfaces whose lifetimes are somewhat shorter than those observed. The model also predicts that more intermediate mergings occur than seems to be the case. It should be noted on comparing figures 16 and 17 that the initial growth of each layer, though plainly visible in the model results, are not well resolved by the experimental data.

6.4. *Variation of Q*

In the attempt to get satisfactory agreement between the model and the experiment we have concentrated mainly on one value of Q. As Q increases, the stability of the system increases, and it is of interest to see what effects this may have on the convection.

Figure 18 shows the depth z_f of the top of the convecting region plotted against the elapsed time for four different values of Q. Apart from two values observed at the beginning of two experiments, the data collapse onto a line of slope $\frac{1}{2}$, independent of Q. Figure 19 shows the equivalent model results for four different values of Q. Again the extremely weak dependence on Q is evident. The same straight line as shown on figure 18 is drawn on figure 19 also. We see that there is very good agreement between the model and the experimental results, though the model predicts a slightly larger rate of advance.

As we have noted earlier, the depth of the lowest layer is considerably greater than that of other layers. In fact, there seems to be a tendency for the layer scales to decrease, but to approach a constant value. In the case of $Q = 0{\cdot}03$, for the last mean profile taken ($t = 1916$), we find for the five layers $h_1 = 29{\cdot}0 \pm 1{\cdot}1$, $h_2 = 9{\cdot}0 \pm 2{\cdot}7$, $h_3 = 6{\cdot}1 \pm 2{\cdot}3$, $h_4 = 5{\cdot}4 \pm 1{\cdot}4$ and $h_5 = 2{\cdot}3 \pm 2{\cdot}5$. The fifth layer is still growing at this point and it reaches a size comparable to that of the third and fourth layers.

In view of this fact the mean vertical scale of all the layers formed, excluding the lowest layer, was calculated, for a number of different values of Q. It is denoted by $\bar{h}$ and both model and experimental results are plotted against Q on figure 20. We see that $\bar{h}$ plainly increases with Q. The data are not sufficiently accurate to be certain of the relationship between $\bar{h}$ and Q; the variance about the mean is too large. However the relationship $\bar{h} = 43Q^{\frac{1}{3}}$ is plotted on the same figure and the agreement is seen to be good.

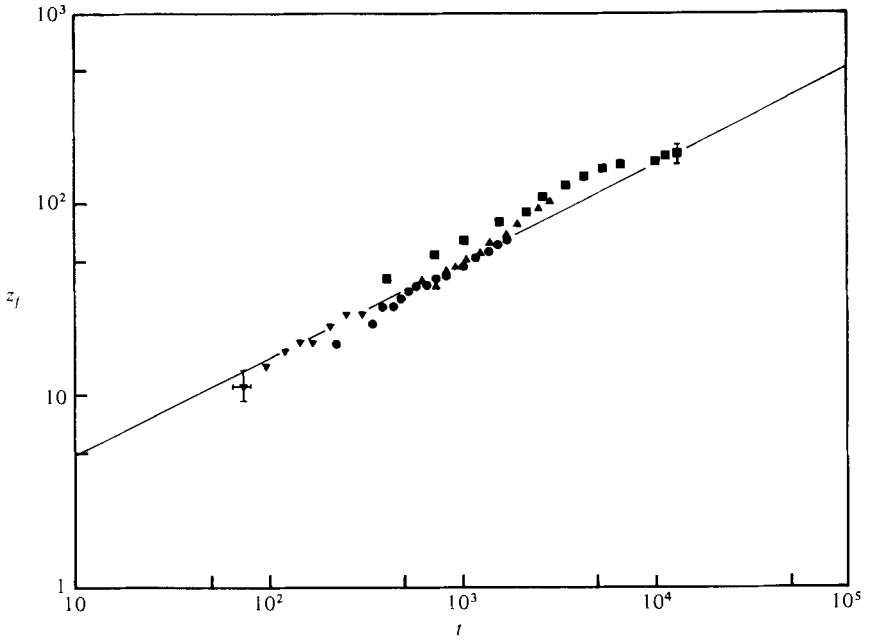

FIGURE 18. The depth z_f of the top of the convecting region plotted on a logarithmic scale against the elapsed time t for the four different experimental values of Q: ▼, $Q = 0{\cdot}010$; ●, $Q = 0{\cdot}030$; ▲, $Q = 0{\cdot}067$; ■, $Q = 0{\cdot}197$. The solid line has slope $\frac{1}{2}$ and is fitted to the data by eye.

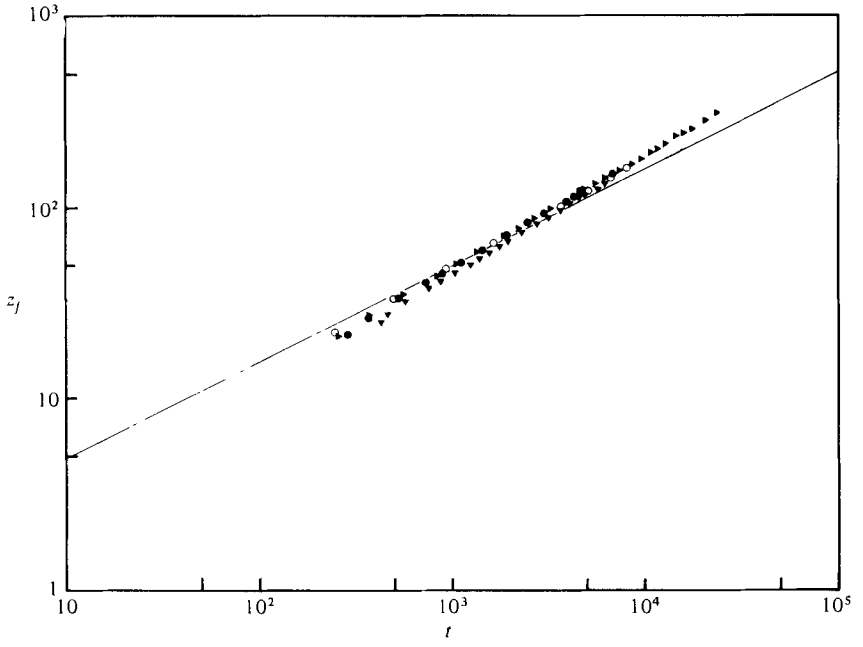

FIGURE 19. The depth z_f of the top of the convecting region plotted on a logarithmic scale against the elapsed time t for the four different theoretical values of Q: ▼, $Q = 0{\cdot}010$; ●, $Q = 0{\cdot}030$; ▶, $Q = 0{\cdot}047$; ○, $Q = 0{\cdot}100$. The same line of slope $\frac{1}{2}$ as plotted in figure 18 is plotted here also.

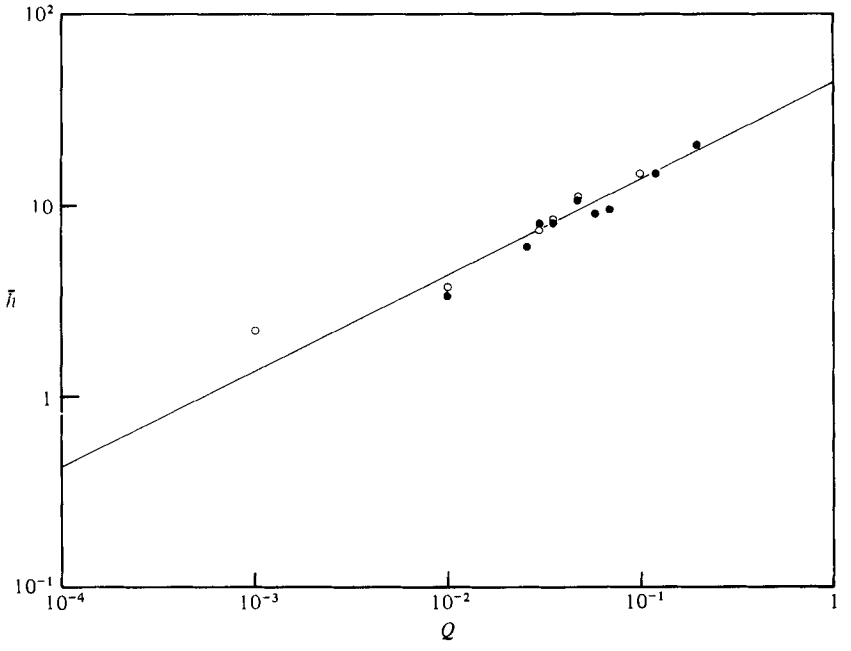

FIGURE 20. The mean thickness, $\bar{h}$, of all layers formed except the first plotted as a function of Q: ●, experimental results; ○, theoretical results. The line $\bar{h} = 43Q^{\frac{1}{2}}$ has been drawn through the data.

7. Discussion

The experiments which compare the convection at different values of the stability parameter Q provide two novel results. The first is that we may approximate the total depth of the convection region z_f by an equation of the form

$$z_f = 1{\cdot}7t^{\frac{1}{2}}. \tag{7.1}$$

In dimensional units this gives

$$\hat{z}_f = 1{\cdot}7H_*^{\frac{1}{2}} S_*^{-\frac{1}{2}} \hat{t}^{\frac{1}{2}}. \tag{7.2}$$

By analogy with thermal conduction we can define an effective conductivity K_T by the relation

$$\hat{z}_f = (4K_T \hat{t})^{\frac{1}{2}}. \tag{7.3}$$

Then from (7.2) we find

$$K_T/\kappa_T = 0{\cdot}72Q^{-1}. \tag{7.4}$$

Thus as Q increases the effective conductivity of the system is reduced, and the system of layers advances more slowly up the water column.

The second result, shown on figure 20, is that the average layer thickness (excluding the lowest layer) is a function of Q and may be approximated by an equation of the form

$$\bar{h} = 43Q^{\frac{1}{2}}. \tag{7.5}$$

In dimensional units this implies

$$h_{\text{average}} = 51\kappa_T^{\frac{1}{2}}(-g\beta d\bar{S}/dz)^{-\frac{1}{4}}. \tag{7.6}$$

Therefore, the average vertical scale of the layers is independent of the heat flux, and depends only on the initial salinity gradient.

We now turn to some more general considerations about these experiments and the model calculations. The calibrations of the model (§ 6.1) gave $R_c = 10000$. This is considerably smaller than the value (24000) found by Turner (1968). There are two reasons for this discrepancy. The first reason is that our estimates of the depth of the first layer used to determine R_c are probably more accurate than Turner's, which were obtained visually by adding dye to the fluid. Our own visual observations showed that it is often quite difficult to see the first layer, or that it is easy to confuse it with the second. Any overestimate of h_1 will lead to a larger value of R_c, and as $R_c \propto h_1^4$ only a small (25 %) discrepancy is needed to account for the difference between the two values. A second reason is that in the present model the increase in α with temperature is included. This means that, for a given temperature step, the value of ΔT is greater than in Turner's calculations, and so the first layer in the present model is deeper at an equivalent time. As the model is calibrated on the layer depth, this implies that we have a smaller value of R_c for the same layer depth.

It is also of interest to note that the value of R_c obtained from estimating when the second layer is initiated is 6500. This is about ten times the critical value obtained from linear theory of the stability of constant, vertical gradients between stress-free boundaries. Consequently, the results of linear stability theory should only be applied to these more complicated situations with caution. For example, in this model the stability criterion (2.9) is appropriate for a fluid with a diffusivity ratio $\tau \ll 1$. In the case where the two components have comparable diffusivities (e.g. an aqueous solution of two solutes) it might then be tempting to use the more general stability criterion involving τ explicitly (see Turner (1973, p. 255)); the present experiments give no indication of whether such a step would be justified.

Similar remarks apply to the role of the Prandtl number in (2.9). In the present calculations $\sigma/(\sigma+1)$ was set at the value appropriate to water at room temperature. Calculations showed that the model was fairly insensitive to the exact value of $\sigma/(\sigma+1)$ provided it was not small. However, it should be emphasized that the experiments were run with only one fluid, and so the appropriateness of using $\sigma/(\sigma+1)$ as the coefficient of R_S in (2.9) as suggested by linear theory has not been tested.

The agreement between the experiments and the model is encouraging, as it implies that it is justifiable to use the empirical flux laws obtained by Turner (1965) to describe the transport across the interfaces. It was not obvious that this would be the case as Turner's measurements were made in quasi-steady conditions by measuring the fluxes across a single interface between two layers. In the present experiments each layer is bounded above and below by an interface, and the depths of the layers are not constant. New layers are being formed and old ones destroyed and the whole system is evolving with time.

We did, however, note some differences in detail between the model and the experiments and, as figures 11, 12 and 13 show, we could get significantly better agreement by altering Turner's flux laws slightly. To carry out a systematic study of the implications of different forms of the flux laws, or to measure the fluxes directly whilst the experiment is in progress are daunting tasks. We have not attempted either of them.

The comparisons of the temperature profiles shown on figures 11, 12 and 13 do show that the model profiles are quite sensitive to the position of the 'knee' – the

value R_ρ^*, above which the ratio of the salt flux to heat flux is constant, and below which it increases with the salt flux, equalling the heat flux when $R_\rho = 1$. Turner's (1965) data place the value of the knee at $R_\rho = 2$, but more recent work (Linden 1974) has indicated that it may be a function of the stability of the interface. Crapper (1975) finds values as low as $R_\rho^* = 1{\cdot}6$ whilst Marmorino & Caldwell (1976) present data which suggest that at very low interface stabilities the position of the knee may be considerably greater than $R_\rho^* = 2$. In view of this uncertainty we have not pursued our investigations of the effect of altering the position of the knee further.

In summary, we conclude that it is possible to build a one-dimensional model of the evolving layers using the assumptions outlined in §3. The experiments we have carried out confirm many of the detailed predictions of the model. The layers increase in number like the square root of time, as does the depth which they occupy. The mean thickness of the layers, excluding the bottom one, appears to be independent of the applied heat flux and inversely proportional to the quarter power of the salinity gradient.

Appendix

The purpose of this appendix is to indicate that in order to construct a workable one-dimensional model it is necessary to neglect the flux of heat across the advancing front when calculating the heat budget for the N layers. Such a procedure leads to the relationships (3.5) for the Nth layer. Substituting (3.5c) into (3.5a) and subtracting (3.5b) from the result, we obtain

$$2h_N \frac{dh_N}{dt} = \phi_{N-1} - \psi_{N-1}. \tag{A 1}$$

The right-hand side of this equation is positive, except for the special case when the density difference across interface $N-1$ is zero. Thus, except under this special circumstance (not encountered in any of our numerical or laboratory experiments), the depth of the last layer monotonically increases, and fluid is being constantly entrained into the convecting layers across the advancing front.

If the flux across the front is not neglected in calculating the heat budget for the layers, (3.5a) is replaced by

$$h_N \frac{dT_N}{dt} = \phi_{N-1} + Q \frac{\partial \theta}{\partial z}(d_N, t). \tag{A 2}$$

The second term on the right-hand side of (A 2) represents the instantaneous molecular heat flux across the advancing front. Substituting (3.5c) into (A 2) and subtracting (3.5b) from the result, we obtain

$$(2h_N - T_N)\frac{dh_N}{dt} = \phi_{N-1} - \psi_{N-1} + Q \frac{\partial}{\partial z}\theta(d_N, t) \tag{A 3}$$

in replacement of (A 1). At t_N^0, the time of initiation of the Nth layer, the last term of (A 3) is infinitely large and negative because of the necessary discontinuity in the temperature profile across the newly formed advancing front. The remaining terms ϕ_{N-1} and ψ_{N-1} are bounded. In the prescription for the initiation of a new layer $h_N = T_N$ [see (3.12)]. Thus dh_N/dt would initially be negative, implying that the last-formed layer detrains for a while after being formed. Calculations indicate that with

time the right-hand side of (A 3) becomes positive and the layer depth then increases. However, the detraining phase is physically unacceptable and a more realistic model results if the heat loss across the advancing front is neglected throughout.

This loss of heat, expressed as a percentage of the total heat input, was small, typically less than 5 %, for all the numerical calculations conducted.

We are grateful to Professor J. S. Turner for stimulating us to work on this problem and for the numerous enlightening discussions we have had with him. We should like to thank Dr Joyce Wheeler for carrying out the numerical computations and producing much of the graphical output presented in the paper. We also acknowledge the assistance of P. Bower-Macer, D. C. Cheesley and D. Lipman with the experiments. The work was partially supported by the Admiralty.

REFERENCES

CHEN, C. F., BRIGGS, D. G. & WIRTZ, R. A. 1971 Stability of thermal convection in a salinity gradient due to lateral heating. *Int. J. Heat Mass Transfer* **14**, 57–65.

CRAPPER, P. F. 1975 Measurements across a diffusive interface. *Deep-Sea Res.* **22**, 537–545.

DEGENS, E. T. & ROSS, D. A. 1969 *Hot Brines and Recent Heavy Metal Deposits in the Red Sea.* Springer.

HUPPERT, H. E. 1971 On the stability of a series of double-diffusive layers. *Deep-Sea Res.* **18**, 1005–1021.

HUPPERT, H. E. & TURNER, J. S. 1972 Double-diffusive convection and its implications for the temperature and salinity structure of the ocean and Lake Vanda. *J. Phys. Oceanog.* **2**, 456–461.

LINDEN, P. F. 1974 A note on the transport across a diffusive interface. *Deep-Sea Res.* **21**, 283–287.

LINDEN, P. F. 1975 The deepening of a mixed layer in a stratified fluid. *J. Fluid Mech.* **71**, 385–405.

LINDEN, P. F. 1976 The formation and destruction of fine-structure by double-diffusive processes. *Deep-Sea Res.* **23**, 895–908.

MARMORINO, G. O. & CALDWELL, D. R. 1976 Heat and salt transport through a diffusive thermohaline interface. *Deep-Sea Res.* **23**, 59–67.

NEAL, V. T., NESHYBA, S. & DENNER, W. 1969 Thermal stratification in the Arctic Ocean. *Science* **166**, 373–374.

NEWMAN, F. C. 1976 Temperature steps in Lake Kivu: A bottom heated saline lake. *J. Phys. Oceanog.* **6**, 157–163.

OSTER, G. 1965 Density gradients. *Scientific American* **213**, 70–76.

SMITH, G. D. 1965 *Numerical Solution of Partial Differential Equations.* Oxford University Press.

TURNER, J. S. 1965 The coupled turbulent transports of salt and heat across a sharp density interface. *Int. J. Heat Mass Transfer* **8**, 759–767.

TURNER, J. S. 1968 The behaviour of a stable salinity gradient heated from below. *J. Fluid Mech.* **33**, 183–200.

TURNER, J. S. 1973 *Buoyancy Effects in Fluids.* Cambridge University Press.

TURNER, J. S. & STOMMEL, H. 1964 A new case of convection in the presence of combined vertical salinity and temperature gradients. *Proc. Natl Acad. Sci.* **52**, 49–53.

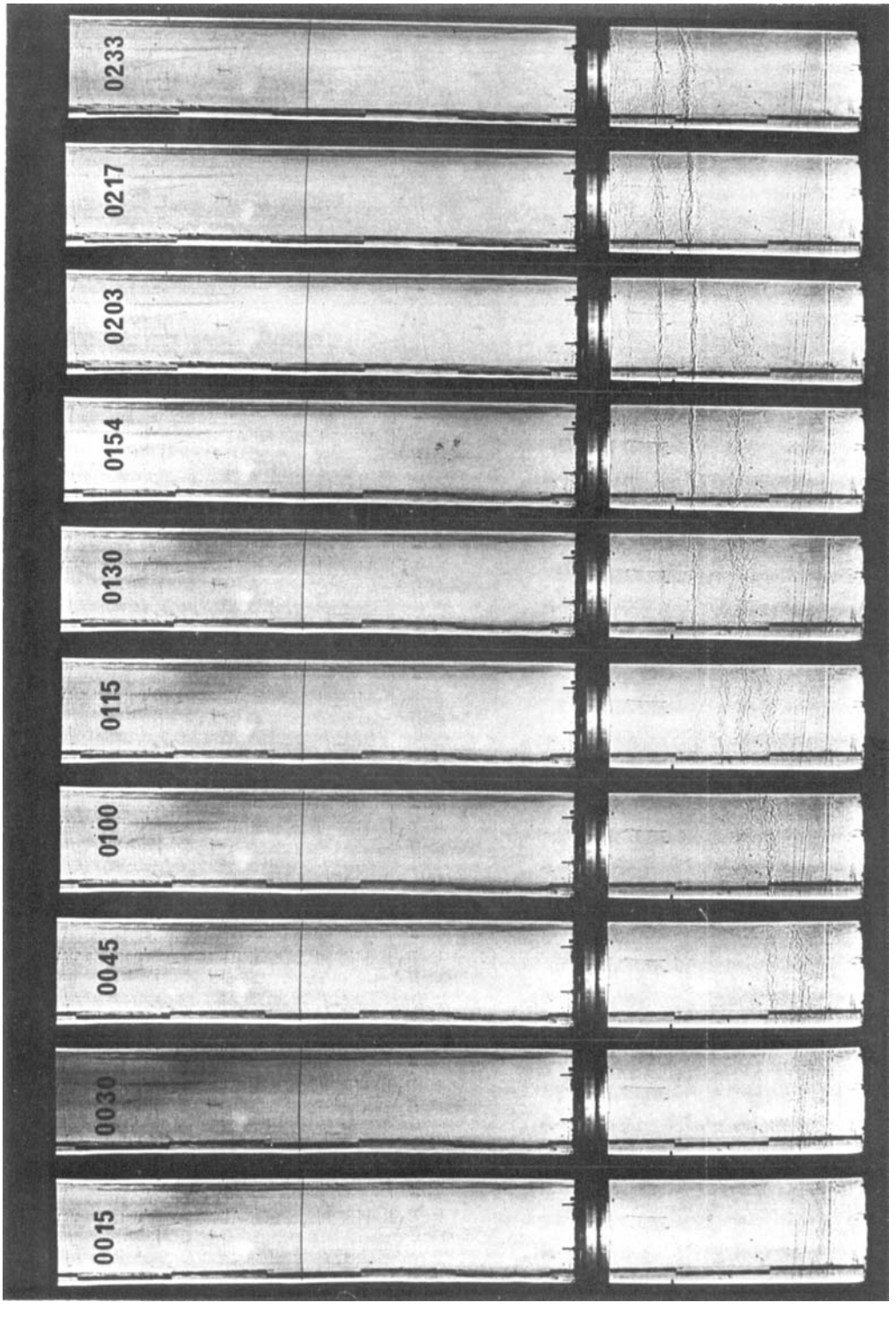

FIGURE 4 (*a*). For legend see plate 4.

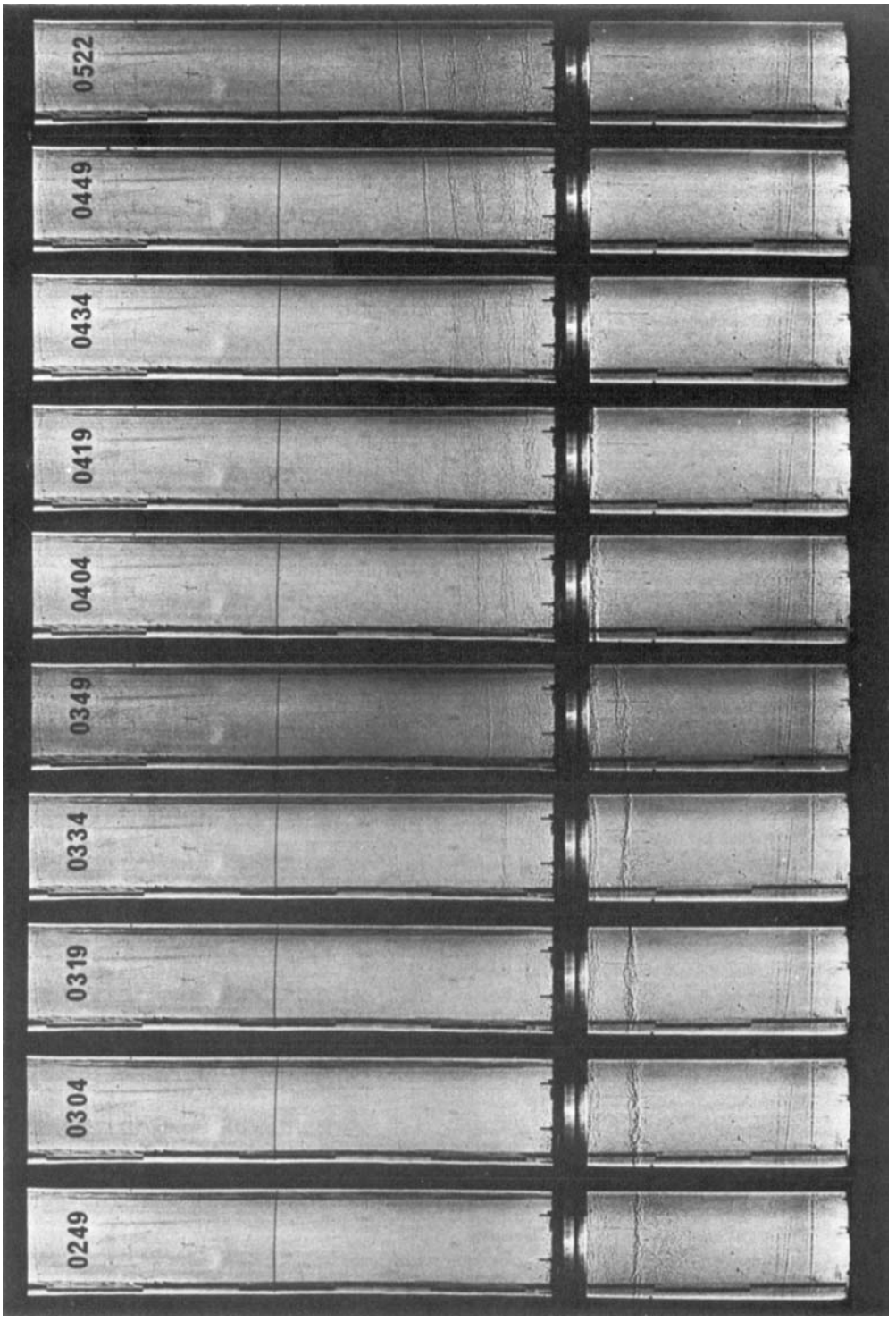

FIGURE 4 (*b*). For legend see plate 4.

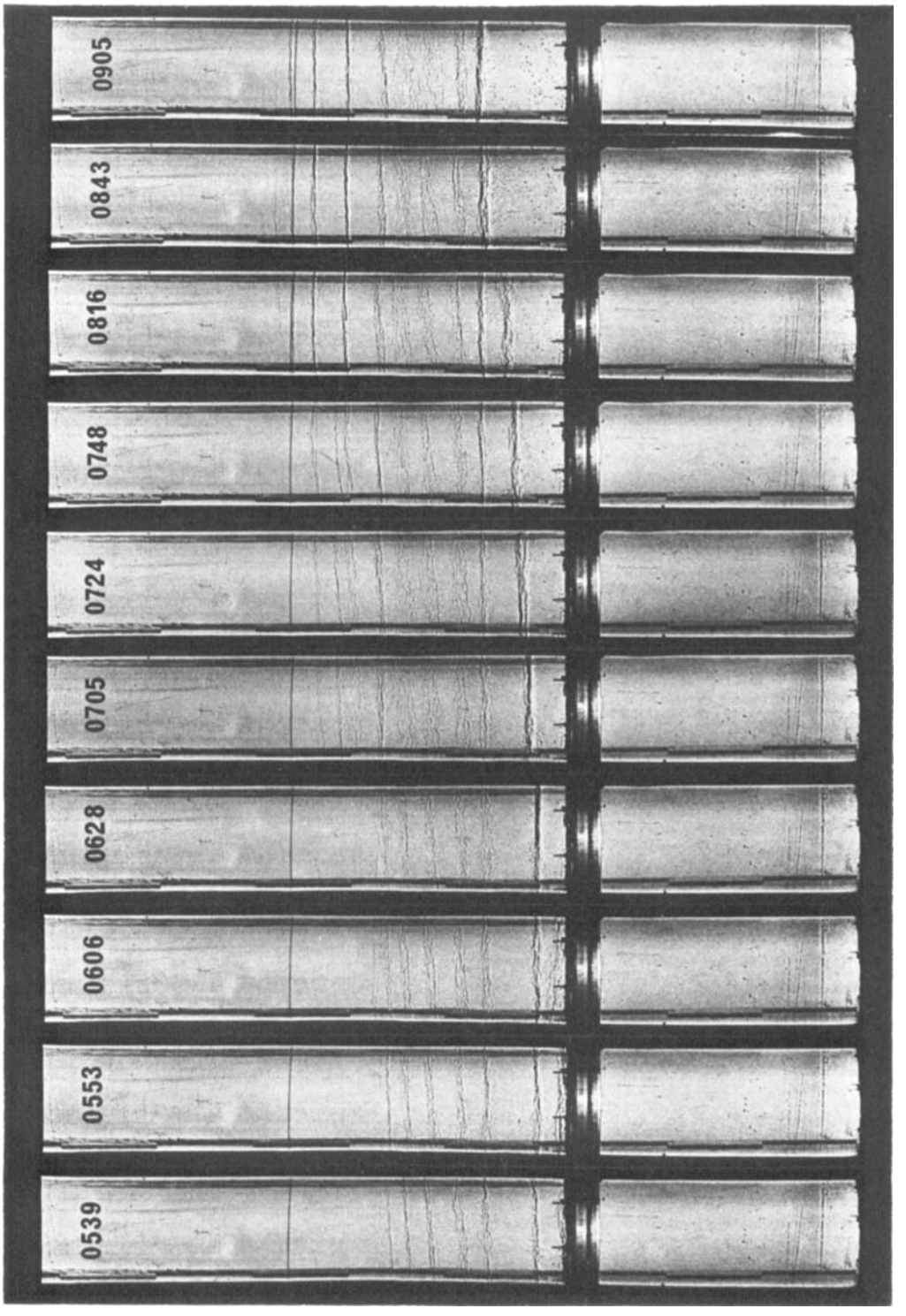

FIGURE 4 (*c*). For legend see plate 4.

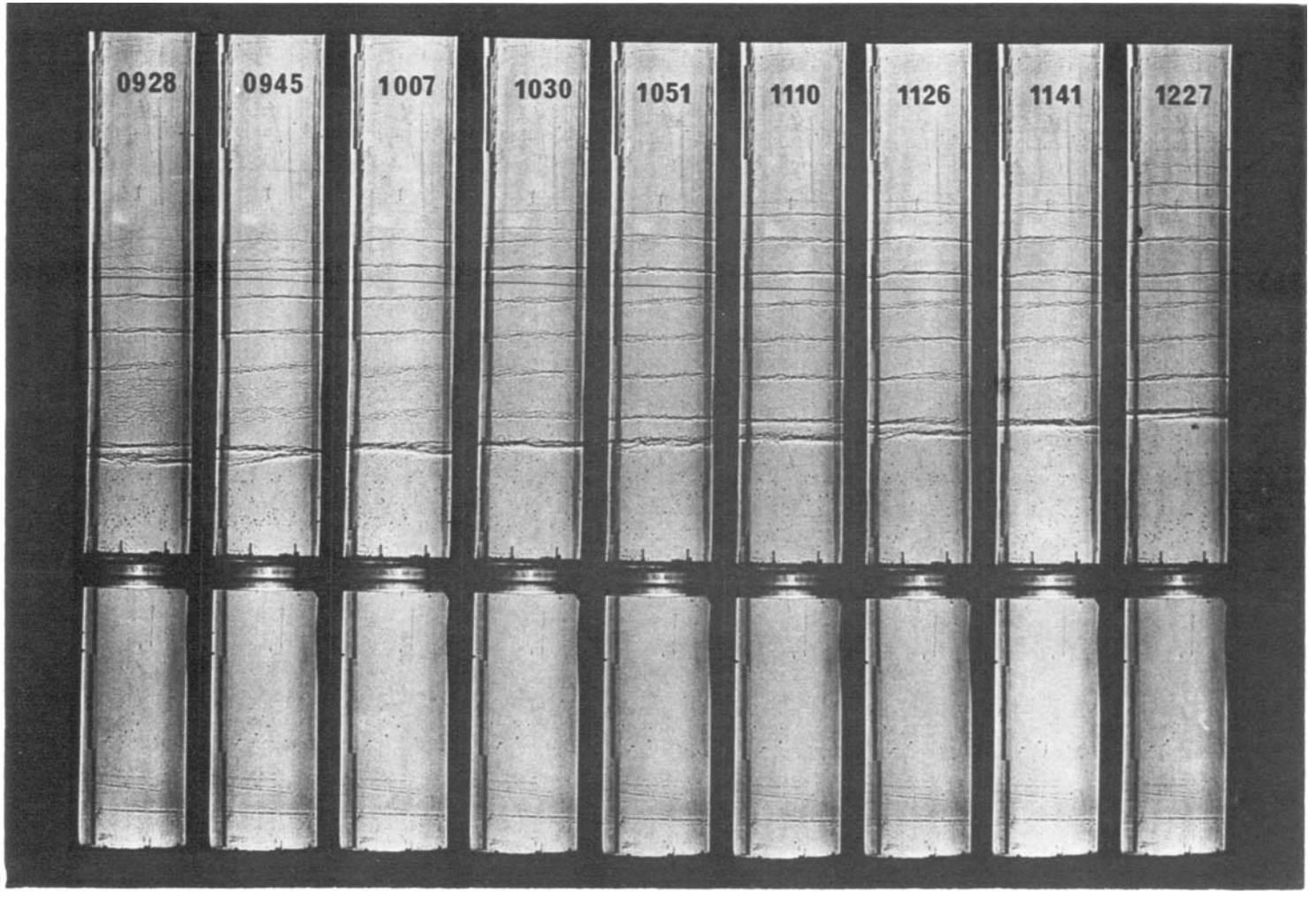

FIGURE 4. Shadowgraphs showing the development of the layered system over a period of 13 h in the deep tank. The photographs were taken sequentially and the time from the start in hours and minutes is indicated at the top of each photograph. The scale visible on the left-hand side of the tank is offset every 10 cm and the base of the tank is about 1·5 cm below the bottom of the visible part of the column. As the tank is cylindrical, on passing through the tank light converges on to a relatively thin vertical strip, giving these shadowgraphs a misleading perspective. The tank is in fact 29 cm in diameter and each interface extends over the whole cross-section. There are several imperfections in the Perspex, which with the join between the small tank and the additional section appear on each photograph.

FIGURE 5 (*a*). For legend see plate 6.

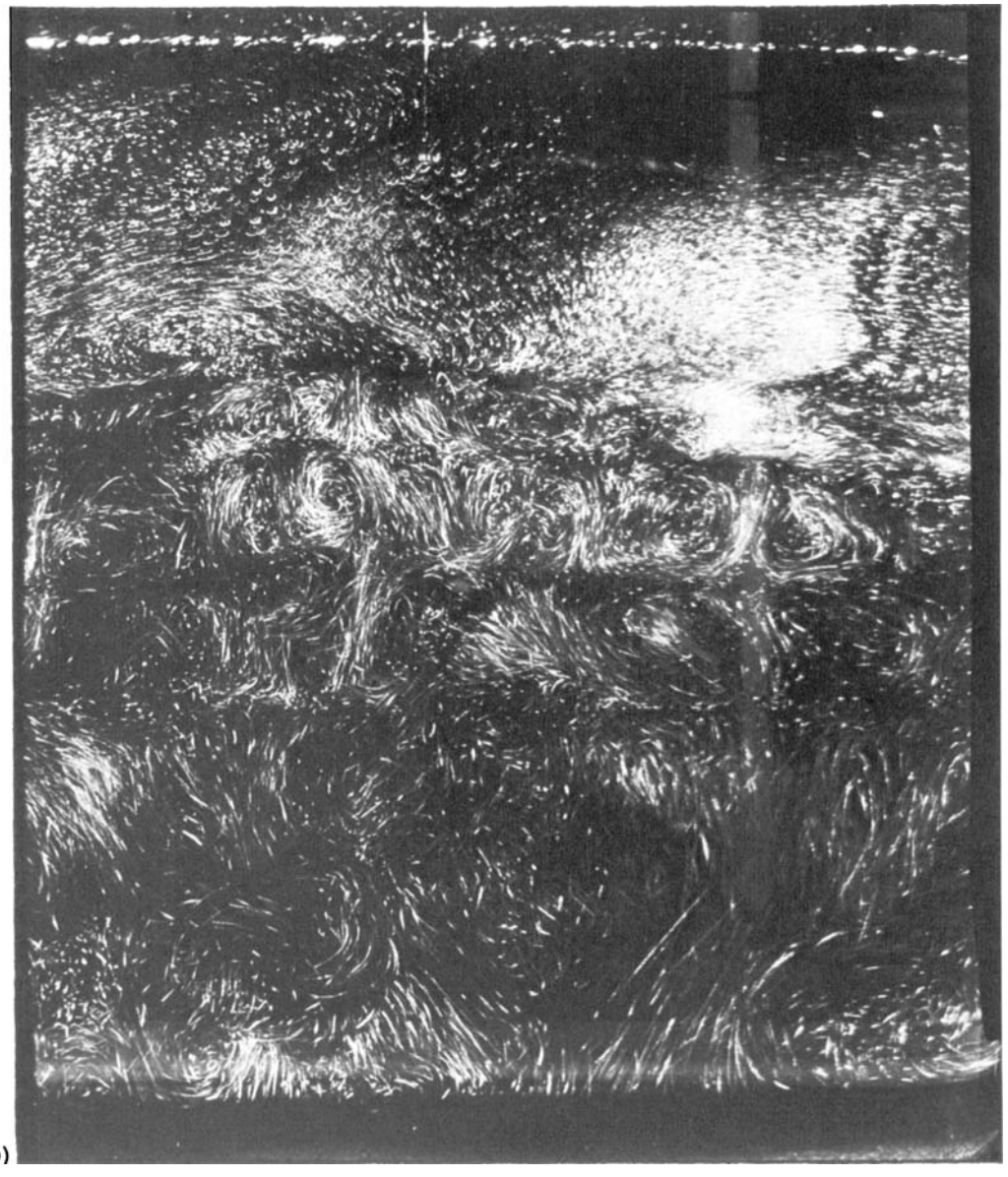

(*b*)

FIGURE 5. Time exposures of aluminium particles suspended in the flow. (*a*) An intermediate stage in the experiment showing about 3 layers. Length of exposure 3 s. (*b*) A later stage in the same experiment with 4 layers. Length of exposure 10 s. Both photographs also show evidence of internal wave motion above the convecting region. The flow is illuminated by a vertical slit of light 1 cm thick and is viewed normal to this beam. The full depth of the tank (25 cm) is visible, except for a region 1·5 cm deep directly above the base.